Antiviral Research 225 (2024) 105856

Contents lists available at ScienceDirect

Antiviral Research

journal homepage: www.elsevier.com/locate/antiviral

Glycan-directed SARS-CoV-2 inhibition by leek extract and lectins with insights into the mode-of-action of Concanavalin A

Maja Klevanski [a,1,*], Heeyoung Kim [b,c,1], Mike Heilemann [d], Thomas Kuner [a,e,2], Ralf Bartenschlager [b,c,f,2]

[a] Department of Functional Neuroanatomy, Institute for Anatomy and Cell Biology, Heidelberg University, Im Neuenheimer Feld 307, 69120, Heidelberg, Germany
[b] Department of Infectious Diseases, Molecular Virology, Heidelberg University, 69120, Heidelberg, Germany
[c] German Center for Infection Research (DZIF), Partner Site Heidelberg, 69120, Heidelberg, Germany
[d] Institute of Physical and Theoretical Chemistry, Goethe-University Frankfurt, Max-von-Laue-Str. 7, 60438, Frankfurt, Germany
[e] German Center for Lung Research (DZL), Partner Site Heidelberg (TLRC), Germany
[f] Division Virus-Associated Carcinogenesis, German Cancer Research Center (DKFZ), 69120 Heidelberg, Germany

ARTICLE INFO

Keywords:
SARS-CoV-2
Antiviral
Virucidal
Lectins
Concanavalin a
Allium porrum extract

ABSTRACT

Four years after its outbreak, severe acute respiratory syndrome coronavirus 2 (SARS-CoV-2) remains a global challenge for human health. At its surface, SARS-CoV-2 features numerous extensively glycosylated spike proteins. This glycan coat supports virion docking and entry into host cells and at the same time renders the virus less susceptible to neutralizing antibodies. Given the high genetic plasticity of SARS-CoV-2 and the rapid emergence of immune escape variants, targeting the glycan shield by carbohydrate-binding agents emerges as a promising strategy. However, the potential of carbohydrate-targeting reagents as viral inhibitors remains underexplored. Here, we tested seven plant-derived carbohydrate-binding proteins, called lectins, and one crude plant extract for their antiviral activity against SARS-CoV-2 in two types of human lung cells: A549 cells ectopically expressing the ACE2 receptor and Calu-3 cells. We identified three lectins and an *Allium porrum* (leek) extract inhibiting SARS-CoV-2 infection in both cell systems with selectivity indices (SI) ranging between >2 and >299. Amongst these, the lectin Concanavalin A (Con A) exerted the most potent and broad activity against a panel of SARS-CoV-2 variants. We used multiplex super-resolution microscopy to address lectin interactions with SARS-CoV-2 and its host cells. Notably, we discovered that Con A not only binds to SARS-CoV-2 virions and their host cells, but also causes SARS-CoV-2 aggregation. Thus, Con A exerts a dual mode-of-action comprising both, antiviral and virucidal, mechanisms. These results establish Con A and other plant lectins as candidates for COVID-19 prevention and basis for further drug development.

1. Introduction

Since the outbreak of the COVID-19 pandemic, more than three quarters of a billion confirmed severe acute respiratory syndrome virus 2 (SARS-CoV-2) infections with a fatality rate of approximately 1% have been reported (as of December 2023) ("WHO Coronavirus (COVID-19) Dashboard," 2023). Moreover, chronic COVID-19-induced illnesses, or long COVID, became an increasing burden to the human population (Huang et al., 2022). As of 2023, only few licensed antiviral drugs are available; and there is only limited or no access to SARS-CoV-2 vaccines, drugs, and tests (Duma et al., 2022; Hashmi et al., 2020) in least developed and low to middle income countries where the majority of the world population resides.

SARS-CoV-2 infection involves binding of the spike (S) protein homotrimer anchored in the envelope of the virus to the angiotensin-converting enzyme 2 (ACE2) receptor on the host cell. The S protein of SARS-CoV-2 is extensively glycosylated with 66 N- and 6 O-glycosylation sites per spike homotrimer (Watanabe et al., 2020). In addition, predictions based on other coronaviruses indicate that also the highly abundant membrane (M) protein residing in the viral envelope carries 8 glycosylation sites (Dawood, 2021). With this large carbohydrate cape the virus efficiently masks potential structures and epitopes for the

* Corresponding author.
E-mail address: maja.klevanski@uni-heidelberg.de (M. Klevanski).
[1] These authors contributed equally in execution.
[2] These authors contributed equally in supervision and conceptualization assistance.

https://doi.org/10.1016/j.antiviral.2024.105856
Received 2 January 2024; Received in revised form 26 February 2024; Accepted 4 March 2024
Available online 5 March 2024

innate and adaptive immune system. At the same time, the glycan shield of the S1 part of the spike protein is crucial for virus' binding and entry into the host cell by conveying certain steric properties to the virus (Casalino et al., 2020; Harbison et al., 2022) and by directly interacting with host receptors (reviewed in: Gong et al., 2021; Lardone et al., 2021; Reis et al., 2021). Recent studies show that the glycosylation state of at least three residues at the receptor-binding domain (RBD) of S1 can substantially affect spike conformation and receptor binding (Casalino et al., 2020; Harbison et al., 2022).

While the overall mutation rate of SARS-CoV-2 is high, glycosylation sites in S are relatively conserved, underlining their role for virion infectivity. Moreover, glycosylation during SARS-CoV-2 maturation affects virion morphology and virus spread (Reis et al., 2021), making the glycosylation shield an attractive target for drug development. Carbohydrate-binding agents such as lectins could (1) render the virus particle more susceptible for antibody recognition; (2) interact with the glycan shield of the virion and/or host receptor, reducing the probability of virus docking and/or host cell entry; and (3) impede virus spread via interfering with glycan-dependent maturation processes.

Lectins are natural proteins that target glycans of high diversity and are widely distributed in all living organisms. Plants feature a large repertoire of lectins that evolved as part of the plant immunity against pathogens. Several lectins exhibit antiviral properties against different viruses, including human immunodeficiency virus, hepatitis C virus, influenza viruses, herpes simplex viruses (reviewed in Mazalovska and Kouokam, 2018), and, importantly, SARS-CoV (Keyaerts et al., 2007; Kumaki et al., 2011). Recent studies related to the effect of plant lectins on SARS-CoV-2 predicted (Barre et al., 2021; Sabzian-Molaei et al., 2022) and unraveled first promising candidates exerting antiviral activity in kidney cells (Liu et al., 2020; Wang et al., 2021), lung epithelial cells (Auth et al., 2021), and in infected rodents (Chan et al., 2022). This underscores the high anti-viral potential of lectins and prompted us to test a panel of lectins to further explore the diverse repertoire of plant lectins. Given that cell type-specific glycosylation differences could tremendously influence treatment efficacy of lectins, we carried out our study using human cell lines relevant for SARS-CoV-2 pathology and used full virus assays reflecting virus replication under physiological conditions.

Recent advances in super-resolution microscopy can visualize the nanostructure of cells and viruses with 10–20 nm localization precision, yet only few studies employed super-resolution methods to provide insights into SARS-CoV-2 inhibition (Cortese et al., 2020; Storti et al., 2021; Wang et al., 2022) and infection pathways (Cortese et al., 2020; Scherer et al., 2022). We took advantage of direct stochastic optical reconstruction microscopy (*d*STORM) (Heilemann et al., 2008) to directly visualize SARS-CoV-2 virions and their interaction with target cells in the presence of seven plant lectins and one plant extract against SARS-CoV-2. Furthermore, we examined the potency of these lectins to interfere with SARS-CoV-2 infection in two human lung epithelial cell lines and addressed the mechanism of action of selected lectins using time-of-addition experiments. Our data acquired by viral assays and aided by *d*STORM analysis demonstrate the potential of plant lectins as antiviral agents to reduce SARS-CoV-2 infection.

2. Materials and methods

2.1. Lectins and other antiviral substances

Concanavalin A (Con A), *Hippeastrum hybrid* agglutinin (HHA), *Morus rubra* lectin (MRL), *Narcissus pseudonarcissus* agglutinin (NPA), *Pisum sativum* agglutinin (PSA), *Urtica dioica* agglutinin (UDA), wheat germ agglutinin (WGA) were purchased from bioWORLD (OH, USA: 22070010, 21510863, 21511394, 21510256, 21510009, 21511038, 21510011). Remdesivir (MedChemExpress, NJ, USA: HY-104077) served as a control in virus inhibition assays. The *Allium porrum* (AP) extract was prepared as described below.

2.2. Preparation of Allium porrum extract

For the crude leek extract, (1) leek sprouts grown until bolting or (2) fresh leek purchased in a grocery store (REWE, Cologne, Germany: 8311846) were used. Stalks, bulbs, and leaves of the bolting leek or leaves of the purchased leek (100 g) were plunge-frozen in liquid nitrogen and grinded using a food processor (Bosch, Stuttgart, Germany: MaxoMixx MS8CM6120). Blended powder was brought to a temperature of 4 °C and squeezed through a sterile cheese cloth. During the squeezing process, 40 ml of ice cold 20 mM Tris with 60 mM NaCl (pH 7.3) was added resulting in 100 ml extract in total. After AP extract was centrifuged at 13,000 rpm at 4 °C for 15 min, the supernatant was filtered through 0.22 μm sterile filters (Merck Millipore, Darmstadt, Germany: S2GPU05RE). For application in virus assays, leaf extract was used due to (1) its high APA contents and (2) its relatively low alliinase activity (Peumans et al., 1997) that is undesirable for our experiments as it could degrade a substantial amount of the lectin. The relatively low alliinase to lectin ratio in leek leafs may also be reflected in SDS gels shown in our study (Fig. S1D) with the bands for the leaf extract being rather confined compared to the more diffuse appearance in the bulb extract lane, which could indicate a higher activity of the alliinase peptidase resulting in various degradation products. To further reduce the amounts of the undesired homodimeric 110 kDa alliinase, the leek filtrate was additionally passed through 100 kDa centrifugation filters (Merck Millipore: UFC910096) , at 4000 rpm for 40 min. The concentration of the resulting leek filtrate was increased to 4 mg/ml or 17.2 mg/ml using 3 kDa concentrators (Sartorius, Göttingen, Germany: VS0192). Leek extract concentrations were evaluated using Bradford assay reagent (Sigma, MO, USA: B6916) at the spectrophotometer (Nanodrop, 2000c; Thermo Scientific, IL, USA). The extraction and purification process is illustrated in Fig. S1A–C.

2.3. Purification of Allium porrum agglutinin (APA)

To prove that the most prominent bands around 12.5 kDa, 25 kDa, 37.5 kDa, and 50 kDa correspond to the *Allium porrum* agglutinin (APA) monomeric, dimeric, trimeric, and tetrameric form, respectively, we performed affinity chromatography using a mannose column. For purification, fresh leek from the grocery store was used. All extraction steps up to the filtration through the 0.22 μm filters were performed as described above (Preparation of *Alliium porrum* extract). The leek filtrate at pH 6.4 was subjected to affinity chromatography. The Enco-Pac chromatography column (Bio-Rad Laboratories, CA, USA: 732–1010) containing 7 ml Sepapore 4B-CL resin suspension (bioWORLD, OH, USA: 20111005) was washed with H_2O and equilibrated with binding buffer (20 mM Tris, 60 mM NaCl). In total, 20 ml of filtrate diluted in 80 ml binding buffer were applied to the mannose column. Bound glycoproteins were eluted either with D-mannose (bioWORLD: 20840070) and α-methyl-D-mannoside (bioWORLD: 21511337) elution buffer or using 24 ml of 20 mM 1,3-diaminopropane (DAP) elution buffer. Eluates were concentrated to 3 ml using 3 kDa centrifugal filter concentrators (Thermo Fischer Scientific: 88514). D-mannose and α-methyl-D-mannoside eluates were pooled together for SDS-PAGE analysis. Dialysis of mannose and DAP eluates was performed at 4 °C in 3 ml 3,5 K Slide-A-Lyser cassettes (Thermo Fischer Scientific: 87723) in five 2 h dialysis steps, each using 500 ml fresh 20 mM Tris pH 7.4. Concentrations of eluates and dialyzed eluates were evaluated using Bradford assay reagent at the spectrophotometer.

2.4. SDS-PAGE

SDS-PAGE was done on 4–20% and 8–16% (w/v) polyacrylamide gradient gels (Bio-Rad Laboratories: 4561094, 4561104). The procedure was carried out as described by Laemmli (1970) using a Bio-Rad PowerPac HC apparatus and Bio-Rad Mini-Protean Tetra System. Electrophoresis was conducted at currents of 10–20 mA for 60 min.

Subsequently, proteins were stained with Coomassie Brilliant Blue G-250 (Carl Roth, Karlsruhe, Germany: A152.1). Washing was performed using 25% MeOH for 2 h.

2.5. Cell culture of lung epithelial cells and virus stock

Calu-3 cells were obtained from ATCC (VA, USA) and cultured in Dulbecco's modified Eagle medium (DMEM, Life Technologies) containing 10% or 20% fetal bovine serum, 100 U/ml penicillin, 100 µg/ml streptomycin, and 1% non-essential amino acids (complete medium). Human ACE2-overexpressing A549 stable cell line (A549-ACE2) was generated as described in Klein et al. and cultured in complete medium containing 250 µg/ml G418 (Klein et al., 2020).

For virus stock production, SARS-CoV-2 isolated from nasopharyngeal and oropharyngeal swabs of PCR-confirmed SARS-CoV-2 positive patients was amplified in Vero E6 cells and further passaged in Calu-3 cells, aliquoted and stored at −80 °C. Virus titer was measured by plaque assay in VeroE6 cells (Mallm et al., 2021).

2.6. Antiviral assays

A549-ACE2 cells were seeded at 1.5 x 10^4 cells per well, or Calu-3 cells at 3 x 10^4 cells per well in clear 96-well plates (Corning, NY, USA). Next day, cells were treated with lectins or remdesivir as a positive control in 10 different concentrations resulting from three-fold serial dilutions and inoculated with SARS-CoV-2 at multiplicity of infection (MOI) of 1. At 24 h post infection, plates were fixed with 6% of formaldehyde and the extent of virus infection was measured by immunostaining with viral nucleocapsid antibody (40143-MM05, Sino Biological, Beijing, China) diluted 1:1000. Subsequently, absorbance was measured at 405 nm. Values were normalized to those obtained with cells treated with solvent control (complete medium) with or without virus infection.

To determine cytotoxicity of test molecules, cell viability was measured in parallel to the antiviral activity test using CellTiter Glo® Luminescent Cell Viability Assay (Promega, WI, USA) according to manufacturer's instruction without virus inoculation. Values were normalized to those of cells treated with solvent control (complete medium).

2.7. Time-of-drug-addition experiments

Calu-3 cells were seeded at 3 x 10^4 cells per well in a clear 96-well plate (Corning). Next day, cells were treated with 1 µM Con A or 10 µM HHA at designated time points (−1 h, 0 h, 2 h, or 6 h) pre- or post-infection and inoculated with SARS-CoV-2 at MOI of 1. Pre-exposure of Calu-3 cells with the lectins 1 h before inoculation (−1 h) was conducted in two ways: with washing out the lectins after 1 h incubation before inoculation (lectin exposure: 1 h–0 h) or leaving the lectins until cells were fixed (lectin exposure: 1 h–24 h). At 24 h post-infection, plates were fixed with 6% formaldehyde and virus infection was evaluated as described in the previous section. Values were normalized using the untreated control as a reference for 100% infection.

2.8. Lectin and antibody staining for dSTORM

The lectins Con A, PSA, UDA, and HHA were purchased as Alexa Fluor 647 (AF647) conjugates (bioWORLD, OH, USA: 21511462, 21511543, 21511581, 21511503). WGA and Con A (in multiplex experiments) were used as CF680 conjugation (Biotium, CA, USA: 29029, 29020). SARS-CoV-2 S protein was detected using a recombinant anti-SARS-CoV-2 spike protein S1 domain primary minibody (fusion of the single-domain antibody to a rabbit Fc domain) obtained from NanoTag Biotechnology (Göttingen, Germany: N3583) and CF680-conjugated anti-rabbit secondary F(ab')$_2$ fragment antibody (Merck, Darmstadt, Germany: SAB4600362) or an AF647-conjugated anti-rabbit secondary F(ab')$_2$ fragment antibody (Abcam, Cambridge, UK: ab181347). Actin was stained using CF680-labeled phalloidin (Biotium: 00053). Clathrin staining was done using an AF647-labeled CHC17 antibody (Novus Biologicals, CO, USA: NB300-613AF647).

For super-resolution experiments, glass-bottom dishes were coated with poly-L-lysine (Merck: P4832) and Calu-3 cells were seeded as a suspension of 2 × 10^5 cells/2 ml. Next day, Calu-3 cells were infected with SARS-CoV-2 at MOI of 5. At 24 h post-infection, cells were fixed with 4% PFA/PBS for 15 min. Samples were three times washed with Tris buffer (50 mM Tris with 150 mM NaCl) for a total of 15 min. In the first step, samples were stained with the anti-SARS-CoV-2 S1 domain primary minibody (1:200) in Tris buffer for 45 min. After three washing steps for a total of 15 min, the secondary anti-rabbit antibody (1:400) and fluorescently labeled lectins were added for further 45 min. Lectins were supplemented with recommended ions and diluted in Tris buffer as follows: Con A-AF647 (1:20) with 5 mM $CaCl_2$ and 5 mM $MnCl_2$, HHA-AF647 (1:10), PSA-AF647 (1:20) with 5 mM $CaCl_2$ and 5 mM $MnCl_2$, UDA-AF647 (1:20) with $ZnCl_2$, WGA-CF680 (1:400) with 5 mM $CaCl_2$. The staining procedure was followed by three 5 min washing steps. For measurements of lectin signal at SARS-CoV-2 particles, we selected sample areas with isolated virions (without cells).

For multiplex super-resolution experiments, glass-bottom dishes were coated with 0.17 mg/ml fibronectin, and A549-ACE2 cells were seeded as a 2 × 10^5 cells/2 ml suspension, infected and chemically fixed as described for Calu-3 cells. Multiplex experiments were performed according to the previously established maS^3TORM procedure (Klevanski et al., 2020). In brief, one to two targets per round were automatically stained by a pipetting robot at the STORM setup and imaged. After each imaging round, signal was removed via photo-bleaching followed by the next staining round. Fluorescent fiducials were used to align images from different acquisition rounds.

2.9. dSTORM imaging and initial processing steps

3D direct STORM (*d*STORM) images were acquired in 85 mM β-mercaptoethylamine (MEA) in Tris buffer adjusted to pH 8 by addition of 35 mM KOH using a 661 nm laser at high power (~2 kW cm^{-2}) for 20,000 frames with an exposure time of 30 ms. Single-molecule localizations were fitted using rapidSTORM software (Wolter et al., 2010). The STORM setup allows astigmatism-based 3D measurements and dual-color imaging of two spectrally close fluorophores in the far-red range employing a 690 nm dichroic filter. Single-molecule localization data was post-processed using a custom written post-processing software that was used to separate localizations produced by AF647 and CF680 fluorophores, to correct lateral drift, and to merge blinking events that lasted for more than one imaging frame. Further details on the SMLM imaging and processing can be found in our previous publication (Klevanski et al., 2020).

2.10. Clumping experiment

Calu-3 produced SARS-CoV-2 was mixed with Con A in 20 mM Tris buffer supplemented by 5 mM $CaCl_2$ and 5 mM $MnCl_2$ for 10 s. The mixture was applied onto a poly-L-lysin coated glass-bottom dish and incubated at 37 °C for 1 h. Subsequently, for immobilization of virions on the glass surface, the buffer was aspirated and the virions were left for drying for 1 min. Subsequently, the dishes were three times washed with Tris buffer for a total of 15 min. The negative control was treated in the exactly same manner, except that no Con A was added to the virions.

2.11. dSTORM data analysis

For the analysis of lectin signal at SARS-CoV-2 virions, the signal produced by a minibody directed against S1 was semi-automatically segmented in ImageJ. The localization data was analyzed using a custom-written software yielding number of blinking events of different

lectins and S1 antibodies per virion. Background signal of the lectins was evaluated by shifting the selection window by 3000 nm to a random adjacent region lacking S1 signal. Signal used for the lectin versus S1 correlation plots was normalized according to the used fluorophores: as the two fluorophores AF647 and CF680 used in these experiments have different blinking dynamics, we determined the ratio of their blinking behavior and used that factor to normalize S1 minibody anti-rabbit CF680 signal to expected AF647 levels. Analogously, the WGA-CF680 signal was normalized. The diameter of SARS-CoV-2 virions based on fluorophore-labeled S1 antibodies or Con A was measured using line profiles laid through a 2D data cloud with a width of 30 nm rotated by 30° around the center of mass defined based on the S1 signal; the average of the six resulting line profiles was calculated per virion (illustrated in Fig. S5). Only virions with a minimum of 40 blinking events were measured; this is done to avoid measuring incomplete spheres, which could lead to an underestimation of diameter.

For the clumping experiment, an ImageJ script was created to automatically segment virus signal and measure area of the virions and clumps and determine the number of blinking events. Number of virions per area was quantified using the mean number of blinking events determined per isolated virion in negative control experiments. 3D renderings of clustered and non-clustered virions were generated using ViSP software (Beheiry and Dahan, 2013).

3. Results

3.1. Plant-derived lectins and leek extract inhibit SARS-CoV-2 in ACE549-ACE2 cells

We selected seven lectins and one lectin-rich extract from the leek with diverse carbohydrate specificity and tested their effects on SARS-CoV-2 infection of human lung epithelial cells. The initial screening of antiviral activity and cytotoxicity of lectins and the leek extract (for details on extract preparation see Materials and Methods section, Supplementary Note 1, and Fig. S1) was carried out using A549 cells stably expressing ACE2. To determine the antiviral effect of lectins on SARS-CoV-2, we treated infected cells with 10 increasing concentrations of lectins or leek extract and used the established antiviral drug remdesivir as a positive control. Four lectins and the leek extract showed profound inhibition of SARS-CoV-2 replication (Fig. 1A, Table 1, and Fig. S2). Concanavalin A (Con A), a lectin that is one of the most widely used in different research areas, e.g. as a ligand for chromatography of glycans, showed best inhibitory properties. Con A reached a remarkably low half-maximal inhibitory concentration (IC_{50}) at 1.39 ± 1.45 μg/ml (≈13 nM) with a half-maximal cytotoxic concentration (CC_{50}) above 416 μg/ml (4 μM) resulting in a selectivity index ($SI=CC_{50}/IC_{50}$) of >299 (Fig. 1B). *Hippeastrum hybrid* agglutinin (HHA), *Urtica dioica* agglutinin (UDA), and *Morus rubra* lectin (MRL) also showed antiviral activities with IC_{50} values of 56.25 ± 68.43 μg/ml, 9.57 ± 3.71 μg/ml, and 167.16 ± 179.77 μg/ml, respectively (Fig. 1A andC, Fig. S2A and B, Table 1). *Narcissus pseudonarcissus* agglutinin (NPA) application resulted in a SI of >32 (Fig. S2C). Strikingly, the crude leek extract (Supplementary Note 1 and Fig. S1) showed a robust antiviral effect with $IC_{50} = 8.76 \pm 3.23$ μg/ml and $CC_{50} > 78$ μg/ml (Fig. 1A and D, Table 1). No measurable antiviral activity in A549-ACE2 cells was found for *Pisum sativum* agglutinin (PSA) and wheat germ agglutinin (WGA) (Fig. 1A, Fig. S2D and E, Table 1) although WGA was previously described as a potent lectin against SARS-CoV-2 (Auth et al., 2021; Wang et al., 2021). Hence, ConA, UDA, and the leek extract effectively inhibited infection of A549-ACE2 cells with Con A demonstrating molar concentrations that are lower than those of remdesivir.

3.2. Cell type-dependent differences in inhibitory activity of lectins on SARS-CoV-2

Our lectin-based approach aims to target the carbohydrate coat of SARS-CoV-2. However, glycosylation of the virus is conveyed by the host cells and diversity of posttranslational modification among different cell types is a well-known phenomenon (Goh and Ng, 2018). Therefore, testing carbohydrate-binding drugs against SARS-CoV-2 produced by different host cell types is mandatory. To identify lectins that could represent universal anti-SARS-CoV-2 drugs, we repeated the antiviral assays in Calu-3 cells endogenously expressing the ACE2 receptor and the transmembrane serine protease 2 (TMPRSS2) (Koch et al., 2021) whose proteolytic activity is required to prime the spike protein for virion envelope fusion with the plasma membrane of the host cell (Jackson et al., 2022). In line with previous studies, showing that Calu-3 cells are less prone to respond to antiviral treatment (Koch et al., 2021; Steuten et al., 2021), most lectins showed diminished or undetectable inhibitory properties against SARS-CoV-2 in Calu-3 cells (Fig. 1, Fig. S2, Table 1). However, Con A, HHA, UDA (in 3 out of 8 experiments), and leek extract maintained antiviral effects, with Con A demonstrating best SI score of up to >174.

3.3. Con A inhibits different SARS-CoV-2 variants

To investigate the potential of lectins against different epidemic variants, we compared the effect of Con A and HHA against the original SARS-CoV-2 strain (B.1) and the Alpha (B.1.1.7), Beta (B.1.351), Delta (B.1.617.2), and Omicron variants (B.1.1.529 BA.1 and BA.5) in A549-ACE2 (Table S1) and Calu-3 cells (Fig. 2, Table S1). Con A exhibited broad antiviral activity against all tested SARS-CoV-2 variants (Fig. 2C, Table S1), including Delta and Omicron. Moreover, when considering the average IC_{50} values pooled across all tested virus variants, an approximately 49-fold lower molar amount of Con A was required to reach a half-maximal inhibitory effect (IC_{50}: 0.05 ± 0.02 μM) compared to remdesivir (IC_{50}: 2.46 ± 2.30 μM), indicating a higher potency.

3.4. Con A and HHA inhibit an early step of the SARS-CoV-2 life cycle

To explore the mechanism by which Con A and HHA inhibit SARS-CoV-2, we applied these lectins at four different time points before, at, or after infection. For this purpose, Calu-3 cells were infected with SARS-CoV-2 at a multiplicity of infection (MOI) of 1. Lectins were applied to the cells 1 h prior to SARS-CoV-2 inoculation and washed away before virus was introduced (−1 h–0 h), or added pre-inoculation and left throughout the experiment (−1 h to end), or introduced simultaneously with the virus (0 h to end), or added 2 h or 6 h post-infection (4 h/6 h to end) and in each of these three cases kept until cell fixation. The measurement of the inhibitory activity of lectins in comparison to infected untreated control cells showed that Con A and HHA effectively inhibited SARS-CoV-2 replication (by 45%–64%) when lectins were added before or at the time of virus inoculation whereas at later time points the antiviral effect vanished (Fig. 3A and B). Additionally, pre-exposure of Calu-3 cells with Con A or HHA for 1 h followed by washing (−1 h–0 h) showed no inhibitory effect. These results suggest that both lectins impeded an early step of the viral replication cycle, most likely virus entry, without interfering with the target cells themselves. A significant inhibitory effect of HHA could be also achieved by post-infection treatment (2 and 6 h after infection).

3.5. Super-resolution imaging of lectin attachment to SARS-CoV-2

We used *d*STORM to visualize whether lectins that showed high (Con A) and moderate (HHA and UDA) inhibitory properties interfere with virus particle binding to cells or virion uptake. We also included lectins with no measurable anti-SARS-CoV-2 properties (PSA and WGA) to the *d*STORM analysis. For PSA, the aim was to clarify whether a lectin that has a similar sugar specificity as Con A but no anti-viral effect would show a different degree of staining or staining pattern at virus particles. For WGA, that represents a lectin with inconsistent anti-SARS-CoV-2 properties ranging from no effect in the present study to a moderate

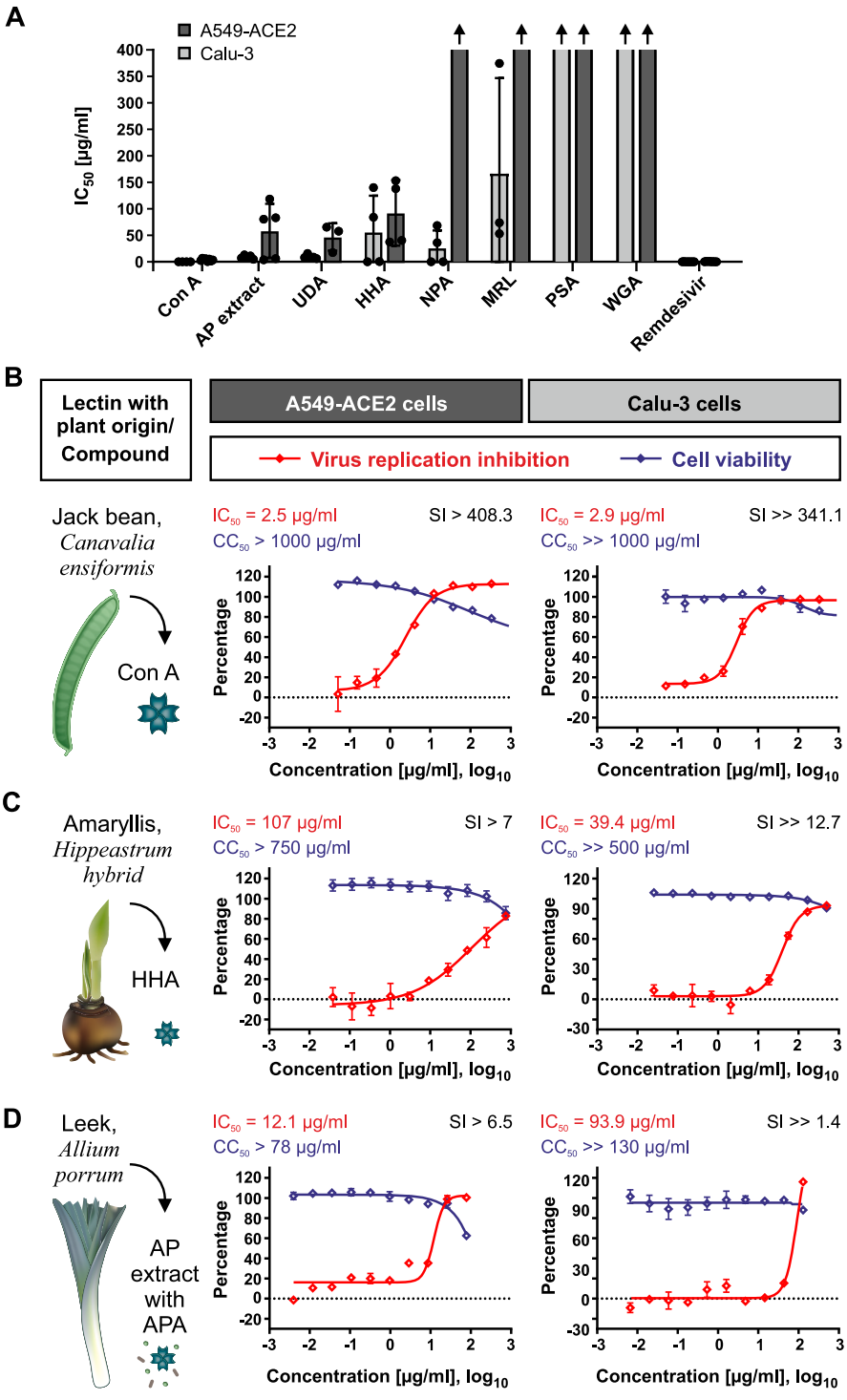

Fig. 1. Antiviral activity of lectins and plant extract against SARS-CoV-2 in two types of human lung epithelial cells. (A) Antiviral activity of seven lectins, the leek extract, and remdesivir (positive control) represented as mean 50% inhibitory concentration (IC_{50}) from individual inhibition curves. A549-ACE2 and Calu-3 cells were treated with serial dilutions of tested compounds and inoculated with SARS-CoV-2, fixed after 24 h, and assessed for virus infection by immunostaining with viral nucleocapsid antibody. Data are shown as mean ± SD. Arrows above individual graph bars indicate instances where lectins at the highest concentration failed to inhibit SARS-CoV-2 infection. (B–D) Representative curves of inhibitory and cytotoxic effect of Concanavalin A (Con A) lectin (B), *Allium porrum* (AP) extract (C), and *Hippeastrum hybrid* agglutinin (HHA) (D) in A549-ACE2 cells (left panels) and Calu-3 cells (right panels). The percentage of inhibition of SARS-CoV-2 infectivity and respective IC_{50} values (B–D) are plotted/denoted in red and the cytotoxic effect with the 50% cytotoxic concentration (CC_{50}) of the substance is represented in blue. Selectivity index (SI) was quantified as CC_{50}/IC_{50} ratio. Each graph shows representative data from two dose-response antiviral activity assays. (A–D) For details on underlying data sets, see Table 1.

Table 1
Antiviral activity of plant lectins against SARS-CoV-2 in A549-ACE2 and Calu-3 cells.

Lectin or substance	MW [kDa]; No of SUs	General glycan specificity	N_1/N_{tot}, N_2/N_{tot}	IC_{50} ± SD [μg/ml]	CC_{50}± SD [μg/ml]	IC_{50} ± SD[a] [μM]	CC_{50} ± SD [μM]	SI from average
A549-ACE2 cells								
AP extract	52; 4[b]	Man	5/8,	8.76 ± 3.23,	>78,	n.q.	n.q.	>8.9,
			3/8	n.a.	>104			n.a.
Con A	104; 4	Man, Glc	4/4	1.39 ± 1.45	>416	0.013 ± 0.014	>4	>299.1
HHA	50; 4	Man, GalNAc	4/4	56.25 ± 68.43	>750	1.13 ± 1.37	>15	>13.3
MRL	52; 1	Gal, GlcNAc	3/4,	167.16 ± 79.77,	>520,	3.33 ± 3.46,	>10,	>3.1,
			1/4	n.a.	>520	n.a.	>10	n.a.
NPA	59; 4	Man	4/6,	26.26 ± 32.80,	842.9 ± 963.3,	0.45 ± 0.56,	14.29 ± 16.33,	~32.1,
			2/6	n.a.	>295	n.a.	>5	n.a.
PSA	53; 2	Man, Glc	1/4,3/4	12.33,	>530,	2.3,	>10,	>43.0,
			3/4	n.a.	>530	n.a.	>10	n.a.
UDA	8.5; 1	Man, GlcNAc	5/6	9.57 ± 3.71	>100	2.74 ± 3.98	>11.77	>10.5
WGA	38; 2	GlcNAc, SA	4/4	n.a.	>360	n.a.	>10	n.a.
RDV	0.6; n.a.	–	8/8	0.15 ± 0.13	>6.02	0.25 ± 0.22	>10	>40.3
Calu-3 cells								
AP extract	52; 4[b]	Man	5/8,	58.45 ± 51.01,	>104,	1.12 ± 0.98,	>2,	>1.8,
			3/8	n.a.	>104	n.a.	>2	n.a.
Con A	104; 4	Man, Glc	4/4,	2.04 ± 1.24,	>260,	0.020 ± 0.012,	>2.5,	>127.4,
			4/4[c]	5.75 ± 0.75	>1000	0.055 ± 0.007	>9.62	>173.9
HHA	50; 4	Man, GalNAc	4/4	92.26 ± 61.82	>500	1.85 ± 1.24	>10	>5.4
MRL	52; 1	Gal, GlcNAc	6/6	n.a.	>260	n.a.	>5	n.a.
NPA	59; 4	Man	4/4	n.a.	>295	n.a.	>5	n.a.
PSA	53; 2	Man, Glc	4/4	n.a.	>265	n.a.	>5	n.a.
succ-Con A	52; 2	Man, Glc	4/4[c]	23.45 ± 8.20	>1000	0.451 ± 0.158	>19.23	>42.7
UDA	8.5; 1	GlcNAc	3/8,	46.99 ± 25.88,	>100,	5.53 ± 3.05,	>11.77,	>2.1,
			5/8	n.a.	>42.5	n.a.	>5	n.a.
WGA	38; 2	GlcNAc, SA	4/4	n.a.	>180	n.a.	>5	n.a.
RDV	0.6; n.a.	–	8/8	0.37 ± 0.25	>6.02	0.62 ± 0.42	>10	>16.4

Mean IC_{50} and CC_{50} values and respective standard deviations (SD) were calculated for the total number of experiments (N_{tot}) or, if pooled quantification was not possible, for data subsets (N_1, N_2). SI was calculated as mean CC_{50} divided by mean IC_{50}. Molecular weight (MW) is provided according to the estimated number (No) of lectin subunits (SUs) predominantly found under experimental conditions.

[a] Molar concentration is calculated according to the No of SUs and MW stated in this table.

[b] For the crude AP extract, MW refers to the lectin *Allium porrum* agglutinin (APA). Note that molar concentration is not quantifiable (n.q.) for the leek extract as it represents a mixture of multiple molecules.

[c] For the purpose of direct comparison between unmodified Con A and succinylated Con A, the data (sub)sets were acquired in a pairwise manner. AP: *Allium porrum*, Con A: Concanavalin A, HHA: *Hippeastrum hybrid* agglutinin, MRL: *Morus rubra* lectin, NPA: *Narcissus pseudonarcissus* agglutinin, PSA: *Pisum sativum* agglutinin, UDA: *Urtica dioica* agglutinin, WGA: wheat germ agglutinin, RDV: Remdesivir. Gal: galactose, GalNAc: N-acetyl galactosamine, Glc: glucose, GlcNac: N-acetyl glucosamine, Man: mannose, SA: sialic acid, n. a.: not available.

(against SARS-CoV-2 pseudovirus in Huh7 cells) or strong inhibitory effect (against different SARS-CoV-2 variants in Vero B4 and Calu-3 cells) in previous studies (Auth et al., 2021; Wang et al., 2021), we aimed to clarify whether super-resolution investigations could explain these inconsistencies. Staining was performed using a primary minibody against the S1 domain of the S protein combined with a secondary F $(ab')_2$ antibody and lectins. Both, the secondary antibody and the lectin were conjugated to the photoswitchable fluorophores Alexa Fluor 647 (AF647) or CF680 (Fig. 4A). Dual-color *d*STORM imaging of virions produced by Calu-3 cells revealed individual S1 minibody-stained SARS-CoV-2 virions, with an unstained core visible in many examples (Fig. 4B, insets). The high number of blinking events for Con A (44 ± 22), PSA (44 ± 20), and WGA (149 ± 88) in the S1-positive area suggests multiple bound lectin molecules per virion (Fig. S3A). Virion-specific signal of these three lectins substantially exceeded the background signal arising from lectin binding to the glass surface (Fig. 4B, Fig. S3A). UDA showed particularly low signal, predominantly occurring in areas occupied by virions; although this trend did not reach statistical significance. Strikingly, despite its anti-viral effect, HHA showed no measurable signal at S1-positive area (Fig. 4B and C and Fig. S3B and C), raising the question of whether it might act via binding to the cells rather than virions. Likewise, the S1 minibody revealed multiple spike proteins of the virion. To quantify colocalization of lectins and spike protein signal, we determined Manders' A and B coefficients using the coordinate-based 3D colocalization approach Coloc-Tesseler (Levet et al., 2019). Our analyses revealed a high degree of overlap between signals of Con A, PSA, and WGA with S1 (Fig. 4C and Fig. S3B and C). The pronounced signal of the mannose-binding lectin Con A at immediate SARS-CoV-2 proximity, supported by the known sugar-specificity of Con A against glycosylation types that are present at the spike protein (Barre et al., 2021; Harbison et al., 2022), argues for a direct interaction of Con A with the virion. This is in good agreement with the time-of-addition experiments (Fig. 3A), pointing towards a block of an early step of infection by Con A.

To analyze whether the amount of lectins showing signal at close proximity of SARS-CoV-2 is directly dependent on the number of spike proteins, we plotted lectin signal versus S1 signal per virion. Indeed, regression analysis reveals linear dependencies between Con A and S1

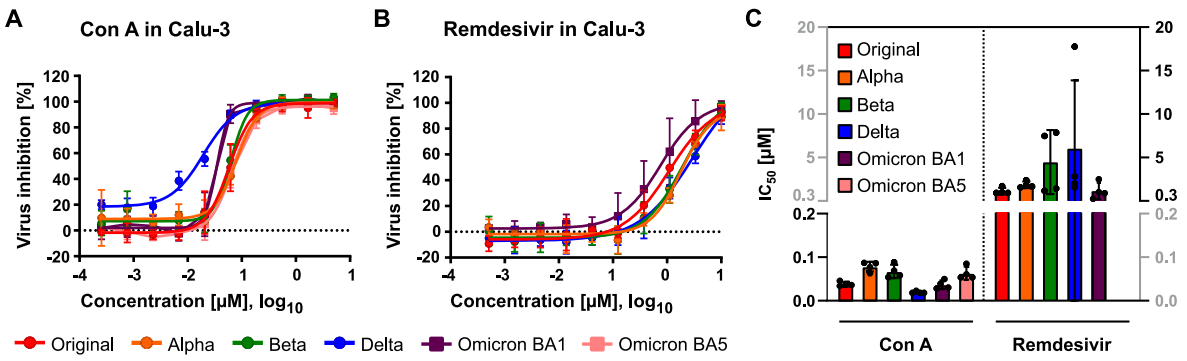

Fig. 2. Con A lectin effectively inhibits infections by six different SARS-CoV-2 variants in Calu-3 cells. (A and B) Treatment efficacy of Con A (A) compared to the control compound remdesivir (B) against six different SARS-CoV-2 variants: the original strain (B.1) and Alpha (B.1.1.7), Beta (B.1.351), Delta (B.1.617.2), and Omicron (B.1.1.529 BA.1 and BA.5) variants. For comparison, concentrations in A and B are plotted in µM. (C) Comparison of 50% inhibitory concentration (IC_{50}) for Con A and remdesivir against different SARS-CoV-2 variants. Data in A, B, and C are shown as mean ± SD from four experiments ($N = 4$). For comparison, taking into account very different molecular weights of Con A and remdesivir, the concentration in this figure is provided in µM with the assumption that Con A is predominantly present as a tetramer.

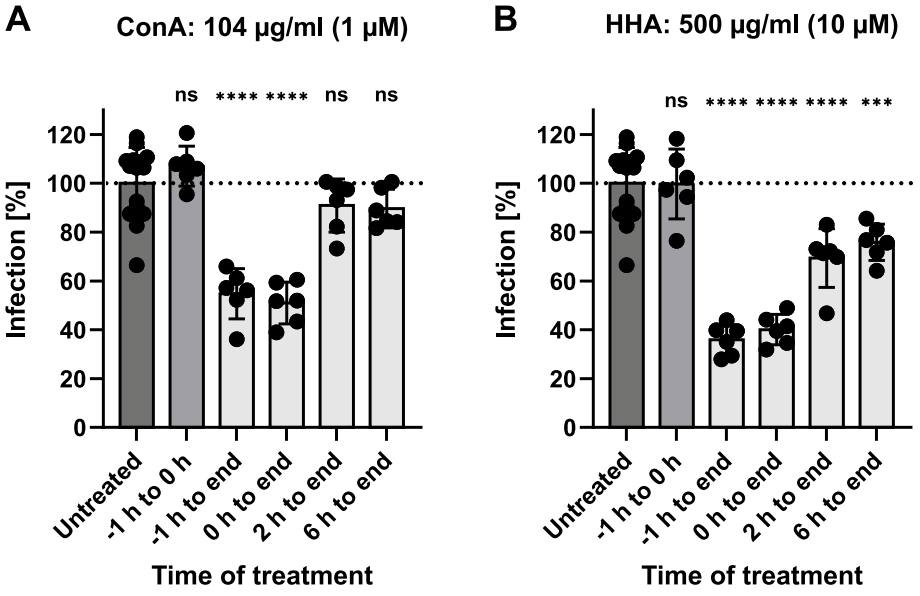

Fig. 3. Time-of-addition experiments using Con A and HHA. (A and B) Inhibition of SARS-CoV-2 replication was evaluated in Calu-3 cells after treatment with Con A (A) and HHA (B) given at different time points before or after infection: 1 h to 0 h, addition 1 h prior and washing out before inoculation with the virus (0 h); −1 h to end, addition 1 h before inoculation until the end of the experiment (24 h post-inoculation); 0 h to end, addition at the time of viral inoculation for the experiment's duration; 2 h/6 h to end, addition 2 h or 6 h post-inoculation for the experiment's duration. Data in A and B are shown as mean ± SD from six to fifteen experiments (untreated $N = 15$, treated $N = 6$). Asterisks denote statistical significance compared to the untreated control group (ns = not significant, ***p ≤ 0.001, ****p ≤ 0.0001; One-way ANOVA with Dunnett's post hoc test).

and PSA and S1 signals (Fig. 4D and E), implicating direct interaction between the spike protein and the tested mannose-binding lectins. By contrast, no obvious correlation between WGA and S1 signals could be observed (Fig. 4F).

To assess possible differences in cell type-specific glycosylation conferred to SARS-CoV-2 particles by the glycosylation machinery of the host cells, we also evaluated binding of fluorophore-conjugated lectins to SARS-CoV-2 virions generated in A549-ACE2 cells. In line with Calu-3-produced virions, we found that Con A colocalized with SARS-CoV-2 particles produced by A549-ACE2 cells (Fig. S4). By contrast, PSA and WGA showed minor signal and HHA was completely absent in S1-positive areas. The minor to absent WGA signal at SARS-CoV-2 produced in A549-ACE2 cells disagrees with the WGA enrichment observed in Calu-3-produced virions (Fig. 4B). This could point towards the high relevance of the host cell in which the virus is produced for WGA binding but does not explain the inconsistent anti-viral activity measured by different laboratories (see Discussion).

By contrast, Con A signal could be detected at SARS-CoV-2 virions produced in both tested cell lines. Therefore, the presumed binding of Con A, which exhibits the strongest antiviral effects, to SARS-CoV-2 virions, was not substantially affected by the cell-specific glycosylation machinery. Taken together, these findings suggest that binding of lectins to the spike protein can explain SARS-CoV-2 inhibition, yet it appears that direct interaction is not the exclusive mechanism at play.

3.6. *Morphometric analysis of lectin-labeled virions*

We also characterized the relative label positions by measuring the diameter of virions labeled by two small antibodies, primary minibody and secondary fluorophore-conjugated $F(ab')_2$ antibody, against the receptor binding domain (RBD) of S1 and the directly labeled Con A. Morphometric analysis of *d*STORM data reveals a mean diameter of

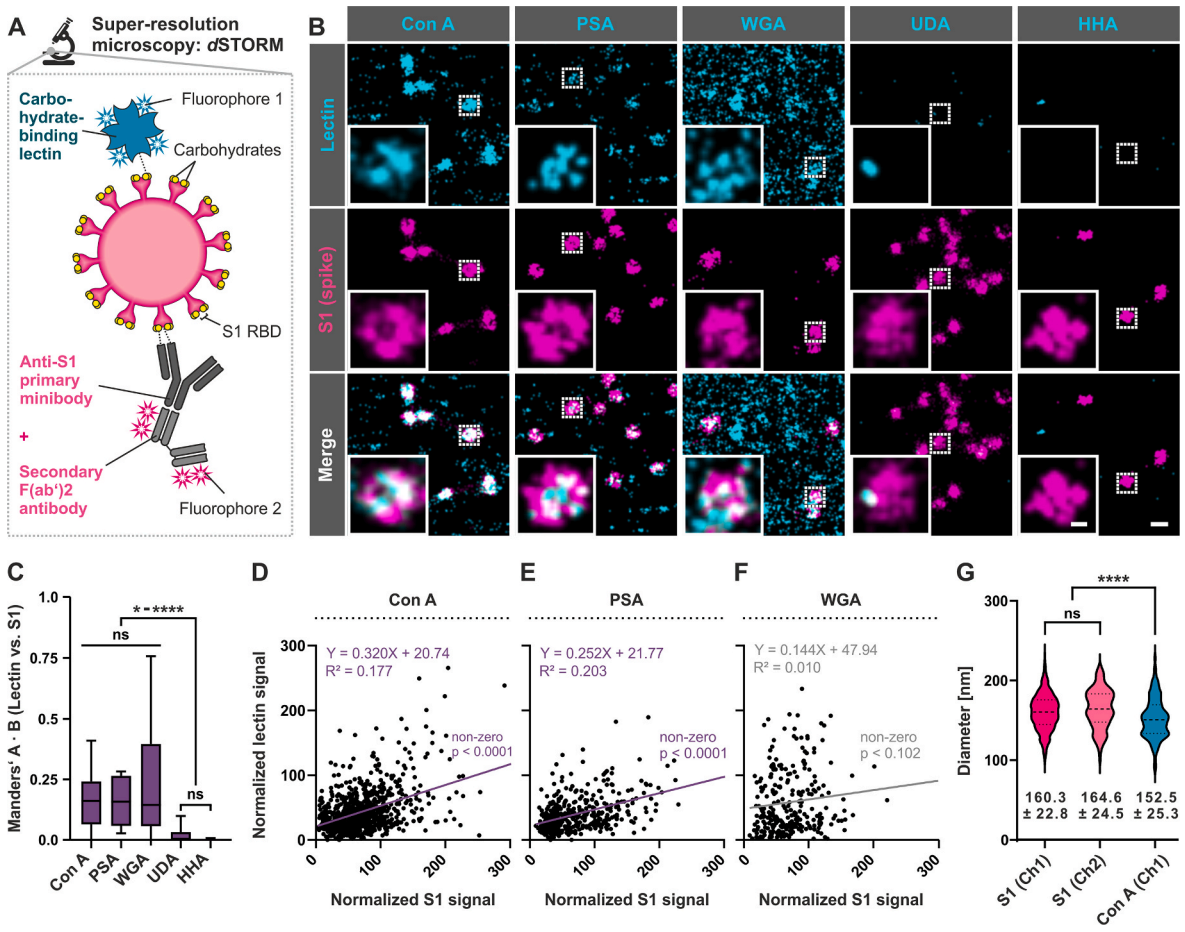

Fig. 4. Visualization of lectin colocalization with SARS-CoV-2 virions using *d*STORM. (A) For the super-resolution microcopy method direct stochastic optical reconstruction microscopy (*d*STORM), SARS-CoV-2 particles produced in Calu-3 cells were stained using small antibodies (minibodies) targeting the receptor binding domain (RBD) of the S1 part of the spike protein and fluorophore-conjugated F(ab)'$_2$ antibodies. Lectins conjugated to fluorophores were used to evaluate their binding to glycosylated regions of SARS-CoV-2 particles. For dual-color *d*STORM, two types of fluorophores were used: Alexa Fluor 647 (AF647) and CF680. Please note, that virus, lectin, cell, and receptor dimensions are not to scale. (B) Dual-color 3D *d*STORM images of SARS-CoV-2 stained with primary and fluorophore-labeled secondary mini-antibodies against S1 region of the spike protein and fluorophore-labeled lectins. Scale bar corresponds to 200 nm in overview images and 50 nm in inserts. (C) Coordinate-based colocalization analysis of lectin and S1 labeling in 3D space using Coloc-Tesseler (Levet et al., 2019). Product between Manders' A and B are represented in a box-and-whisker plot from 4 independent experiments per lectin ($N = 4$) and 4–7 *d*STORM images per experiment ($4 \leq n \leq 7$). (D–F) Correlation analyses between lectin signal and S1 signal. Each dot represents normalized signal per SARS-CoV-2 sphere. Linear regression fitting (purple) confirms correlation between S1 and Con A (D) and S1 and PSA (E) while WGA signal did not show clear correlation with S1 signal (F); unreliable regression fit is shown in gray. (G) The diameter of virions was measured based on rotated line profiles ($N = 4$ experiments per data set, $n = 135$ to 888 virions per experiment). Median values and quartiles are shown in the violin plot. Mean values ± SD are indicated. For more details on STORM analysis, see Materials and Methods section. Asterisks in C and G denote statistical significance of pairwise comparisons between data sets connected by staple-shaped lines or summarized comparisons between all pairs covered by horizontal lines (ns = not significant, *p ≤ 0.05, ****p ≤ 0.0001; ANOVA with Tukey's post hoc test).

160.3 or 164.6 nm (imaged using AF647 or CF680 fluorophores, respectively) and 152.5 nm for the S1- and the Con A-based measurement, respectively (Fig. 4G; for details, see Materials and methods and Fig. S5). These values agree well with previous morphometric data obtained from cryo-electron tomographs that show a mean diameter of 96.6 nm of SARS-CoV-2 without spikes and a length of 22.5 nm for spike trimers that would result in a total diameter of 141.6 nm for virions with maximally extended spike proteins (Laue et al., 2021). The length of the two small antibodies used to detect S1 are expected to measure 12–14 nm in total; and the Con A tetramer is expected to have an extension of maximally 7 nm (PDB ID: 5CNA). Therefore, we would expect a diameter of 167.6 nm for the S1 signal and 155.6 nm for Con A signal in case it would bind the RBD of S1. Hence, the discrepancy between antibody- and lectin-based measurements is expected to be approximately 12 nm. Our *d*STORM-based measurements reveal a difference of 8–12 nm, suggesting that most of the lectin signal is localized at the RBD of the spike protein. These results demonstrate that labeled Con A can be used as a tool in super-resolution microscopy to image individual SARS-CoV-2 particles at their native size. Furthermore, we could demonstrate that *d*STORM is a powerful approach for the study of single-virus particles and the relative position of virion interactors, such as lectins.

3.7. Lectin-based super-resolution imaging of SARS-CoV-2-infected A549-ACE2 and Calu-3 cells

To study SARS-CoV-2 in the context of infected cells and endocytosis, we performed multiplexed 3D *d*STORM experiments (Klevanski et al., 2020) of lectins bound inside or at the surface of A549-ACE2 cells (Fig. 5). These cells exhibit a flatter morphology compared to Calu-3 cells and allowed measurements for selected lectins. Con A, PSA, and WGA showed high signal levels at the cell surface and revealed filopodial protrusions (Fig. 5A–C) of A549-ACE2 cells. Interestingly, HHA did not stain the glycocalyx of A549-ACE2 cells (Fig. 5D).

In addition, to explore potential overlap of lectins with endocytic compartments, we monitored whether lectins showed intracellular

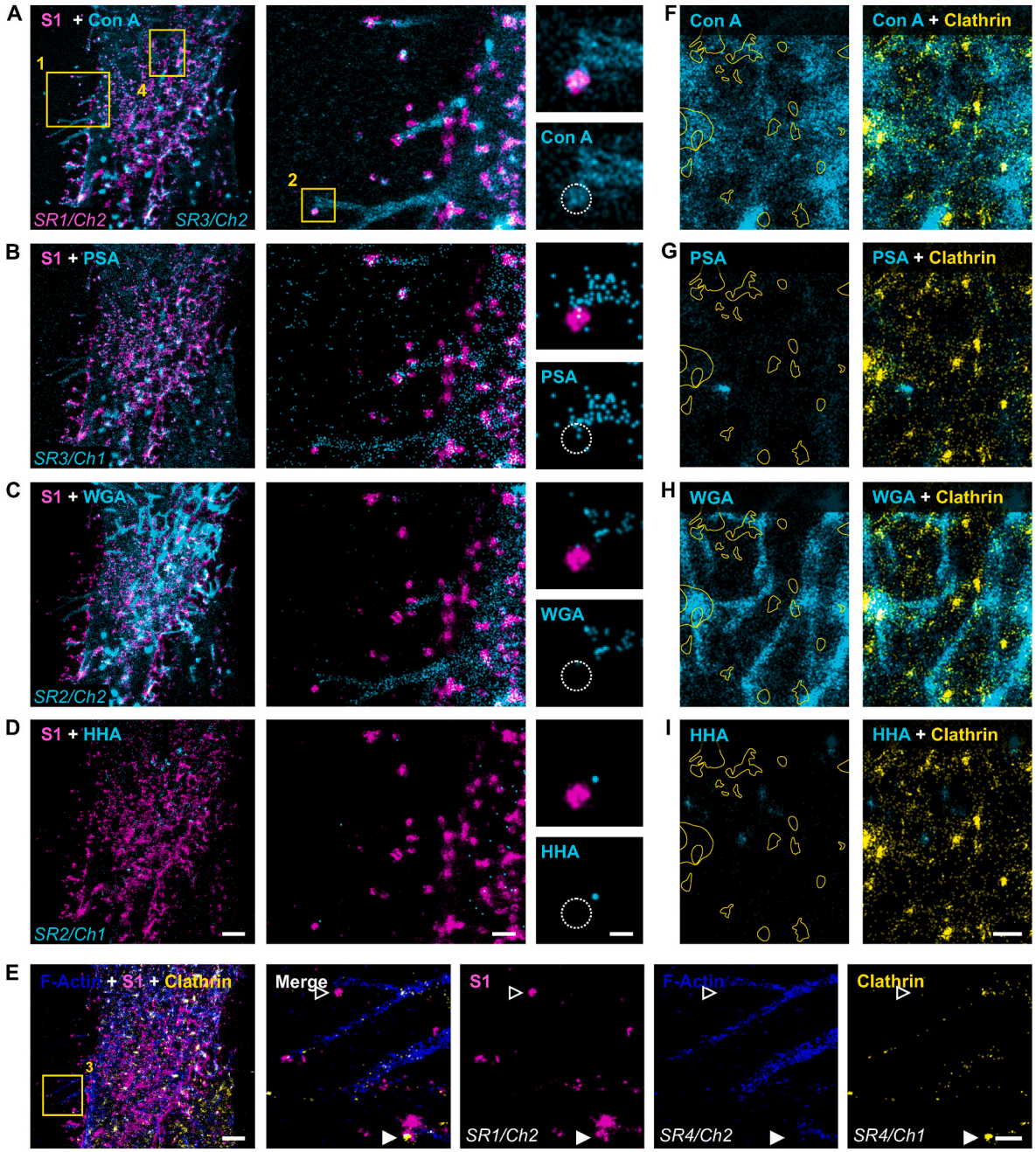

Fig. 5. Multiplexed *d*STORM experiment in SARS-CoV-2-infected A549-ACE2 cells. (A) Pronounced Con A signal in A549-ACE2 cells and in SARS-CoV-2-occupied area (magnified images of boxed region 1 and 2) outlined by a dotted-line circle. (B) PSA shows sparse signal at the cell surface and virions. (C) WGA exhibits no specific binding to virions produced in A549-ACE2 cells; but is enriched at the cell membrane, filopodia, and rod-shaped structures close to the glass-attached plasma membrane (3D image not shown). (D) HHA signal does not colocalize with virions or viruses. (E) Clathrin staining in magnified images of boxed region 3 demonstrates SARS-CoV-2 that presumably undergoes clathrin-mediated endocytosis (filled arrowhead). Other SARS-CoV-2 particles do not show colocalization with clathrin (empty arrowhead) and might represent just exocytosed or docked virions. (F–I) Close-up views (boxed region 4 in A) of lectins at A549-ACE2 cells and their distribution relative to clathrin-enriched regions (outlined by yellow lines). Scale bars correspond to 2 μm in left panels of A-E; to 500 nm in central panels of A-D, magnified panels in E, and all panels in F–I; and to 150 nm in right panels of A-D. Multiplex data of seven targets was acquired in four staining rounds (SR) in dual-color imaging mode with two spectrally discernible channels (Ch) per round.

signals at clathrin-positive areas, the main endocytic pathway predicted for SARS-CoV-2 entry into A549-ACE2 cells lacking TMPRSS2 (Koch et al., 2021). Indeed, *d*STORM imaging confirmed that SARS-CoV-2 entered A549-ACE2 cells via clathrin-mediated endocytosis. S1 minibody staining revealed SARS-CoV-2 particles, which were located at the cell surface and often at the tips of the filopodial protrusions (Fig. 5E). Interestingly, at filopodial protrusions we found two populations of SARS-CoV-2 particles: (1) particles devoid of proximal clathrin signal that might represent budding virions or early stages of virus entry, and (2) particles that coincided with clathrin staining at the tips of filopodia that may represent virus particles that are entering host cells (empty and filled arrowhead in close-up images in Fig. 5E, respectively). The latter observation further strengthens recent findings demonstrating that endocytosis of SARS-CoV-2 can selectively take place at the tips of cellular protrusions (Wu et al., 2023). Both SARS-CoV-2 populations coincided with comparably pronounced Con A staining (not shown),

suggesting that both, entering and budding viral particles possess Con A-susceptible glycosylation at their surface. When examining lectin signal in the cell soma, we observed that Con A, WGA, and to a very low extent PSA, showed only partial overlap with clathrin-coated compartments (Fig. 5F–H). While these lectins were stained rather broadly, HHA demonstrated confined small signal clusters in the cytoplasm (Fig. 5I) that did not overlap with clathrin staining and may reflect small organelles, such as the endoplasmic reticulum-Golgi intermediate compartment (ERGIC), suggesting that HHA might exhibit its intracellular antiviral effect after clathrin-mediated endocytosis of virus particles.

While our *d*STORM data suggested a direct interaction of Con A and SARS-CoV-2 spike protein (Fig. 4), it does not explain how UDA and HHA, neither of which showed quantifiable signal in spatial proximity to the virions, exert their antiviral effect. Therefore, we also examined whether UDA and HHA were able to bind specific structures at the surface of or inside Calu-3 cells. Please note that the sparse signal of UDA and HHA allowed *d*STORM imaging at the voluminous Calu-3 cells while other lectins Con A and PSA resulted in a very dense signal, which precluded reliable dSTORM measurements. Staining of Calu-3 cells with fluorophore-labeled UDA revealed very sparse signals (Fig. S6A–C) with no staining of the glycocalyx. Interestingly, closer examination of SARS-CoV-2-positive areas revealed UDA signal at some virions located in immediate Calu-3 proximity (above or underneath the cell) while most virions located outside the cell-occupied area did not show UDA signal (exemplified in Fig. S6B and C, magnified areas #2 and #3). This suggests a potential binding mechanism that operates within a specific time window when viral surface proteins and host cell receptors interact, triggering structural changes that could create new points of attack for UDA. Evaluation of HHA signal in Calu-3 cells revealed round to oval-shaped HHA-positive clusters with the diameter/minor axis of ~120 nm and the major axis up to 500 nm (Fig. S6E and F), similar to *d*STORM data of HHA in A549-ACE2 cells (Fig. 5I). These clusters did not colocalize with F-actin and Con A. Very little colocalization was observed with WGA, which is known to bind the glycocalyx, trans-Golgi, trans-Golgi network (Vetterlein et al., 2002), and endosomes (Raub et al., 1990) in eukaryotic cells. Further experiments are needed to confirm the specificity of the HHA signal and investigate at which particular organelles HHA could exert its antiviral effect.

3.8. Con A-induced aggregation of SARS-CoV-2

To address whether there is some difference in the inhibition mode of the various lectins, we also determined the Hill coefficient, which reports binding cooperativity, from the neutralization curves that were fitted by the sigmoidal dose-response function (Fig. S8A). Statistical analysis demonstrates that UDA and HHA exhibit Hill coefficients that do not significantly differ from 1, possibly pointing to an independent binding mode. In contrast, Con A demonstrates a Hill coefficient of 1.74 ± 0.41, significantly higher than 1 ($p = 0.007$), suggesting a cooperative

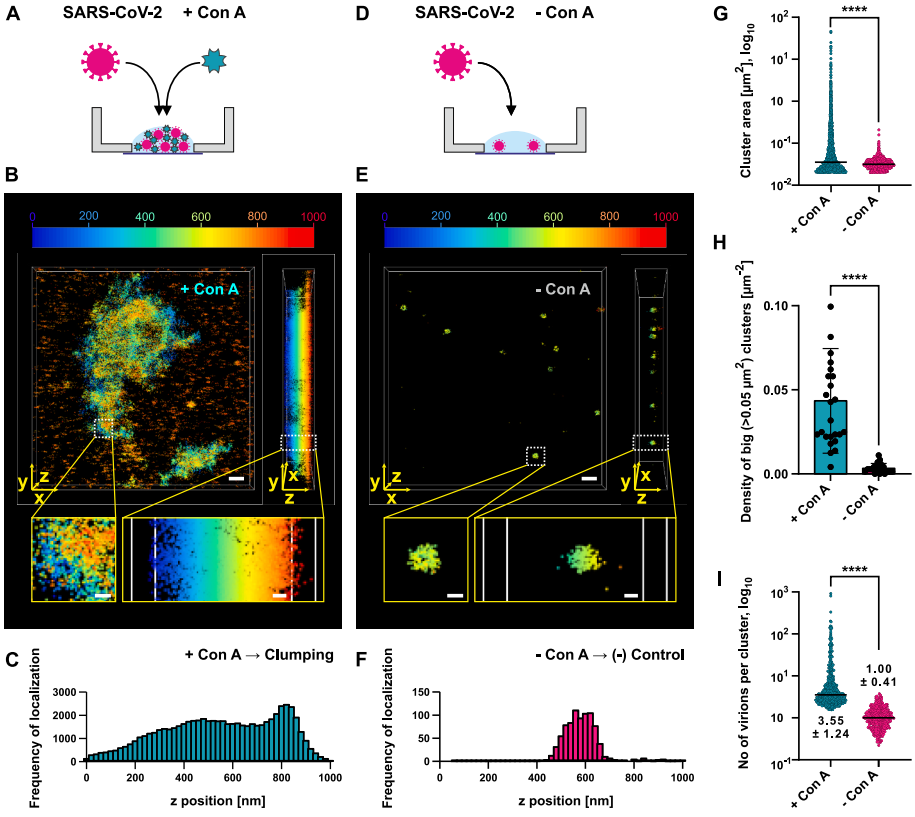

Fig. 6. Con A agglutinates SARS-CoV-2 particles. (A–F) SARS-CoV-2 particles produced in Calu-3 cells were mixed with 0.5 μM (52 μg/ml) Con A in Tris buffer (A–C) or only with Tris buffer without lectin (negative control) (D–F) and applied to a glass-bottom dish for 3D *d*STORM imaging (see Materials and Methods section for detailed experimental setup). 3D super-resolution images demonstrating formation of bulky SARS-CoV-2 clumps upon Con A application (B) while no clumping was observed without lectin addition (E) (rendered using ViSP viewer). Z histograms (corresponding to panels B and E) of Con A-induced SARS-CoV-2 macro-clusters extending into the axial direction (C) and single SARS-CoV-2 spheres (F). (G) Cluster analysis of rendered super-resolution images performed in ImageJ. (H) Density of clusters with a minimal area of 0.05 μm^2. (I) Number of SARS-CoV-2 particles per cluster quantified as number of blinking events in a cluster divided by the median number of blinking events per isolated virion (quantified based on negative control experiments). Scale bars in panels B and E correspond to 500 nm in full lateral view and 100 nm in magnified views. Data points in G represent individual clusters from 20 to 25 images acquired in 4 independent experiments; horizontal bars represent median. Data in H are shown as mean ± SD with individual data points being means from 20 to 25 images acquired in 4 independent experiments. Data in I is based on individual clusters from 5 to 7 images and are represented as median ± MAD. Asterisks in panels G–I denote statistical significance (****$p \leq 0.00001$; Mann-Whiteney *U* test).

binding effect potentially contributing to its antiviral activity. The self-induced binding augmentation can be conferred by the ability of the substance to engage multiple binding sites simultaneously, increasing the likelihood of binding events and/or enhancing the overall binding affinity.

As Con A predominantly forms a multivalent tetramer with high agglutinating properties (Greig and Bouillant, 1977; Kuo et al., 2007), we explored whether Con A could reduce SARS-CoV-2 infectivity by cross-linking the virions. We tested this possibility by 3D *d*STORM imaging of virions incubated with 0.5 μM (52 μg/ml) Con A (Fig. 6A). Indeed, Con A application induced strong clumping of SARS-CoV-2 virions (Fig. 6B and Fig. S7A) reflected in the increased number of clusters with big areas up to 46 μm^2 (Fig. 6G and H). Examination in 3D space revealed that virus–Con A aggregates were formed in all three dimensions (Fig. 6B and C). In contrast, no aggregation was observed for the negative control where no lectin was added (Fig. 6D–H, Fig. S7B). These data support that Con A could bind the spike protein of SARS-CoV-2 and agglutinate the virions resulting in the inhibition of SARS-CoV-2 infection.

We determined the median number of *d*STORM localizations per single virion and quantified the number of virions per aggregate by dividing the number of STORM localizations per aggregate by the quantal localization content of a single virion and obtained the median aggregate size of 3.6 virions (Fig. 6I) with the biggest aggregate consisting of 918 virions. Please note that these numbers may be an underestimation of virion numbers per aggregate due to physical properties resulting from dense aggregation because of the following circumstances. First, the number of penetrating antibodies can be reduced by increased molecular crowding. Second, the number of blinking events that can be recorded for Alexa Fluor 647 is expected to be reduced due to fluorophores that are closer than 10 nm (Helmerich et al., 2022), which is expected in case of multivalent cross-linking by Con A that is smaller than 7 nm.

Furthermore, to explore the relevance of multivalency, we compared the antiviral performance of native Con A with its succinylated variant (succ-Con A) that has lower valency and agglutinating properties (Gunther et al., 1973) in Calu-3 cells. Indeed, in a side-by-side comparison in Calu 3 cells, succ-Con A demonstrated lower performance with an approximately four times lower SI (Fig. S8B, Table 1). Interestingly, in this dataset both Con A and succ-Con A, exhibited an increased Hill coefficient of approximately 3, indicating a similar level of cooperativity (Fig. S8B and C). This indicates agglutination mechanisms for both Con A and succ-Con A.

In summary, we found that Con A showed a substantial anti-SARS-CoV-2 effect at nanomolar concentrations. This inhibitory effect is most likely due to blocking virus entry and a virucidal effect caused by virus clumping.

4. Discussion

Glycosylation of proteins at the surface of SARS-CoV-2 allows the virus to evade our immune system but is also crucial for virus docking and entry (Casalino et al., 2020; Yang et al., 2020; reviewed in Shajahan et al., 2021). Thus, the glycan shield could be seen as the Achilles' heel of SARS-CoV-2 that can be targeted by carbohydrate-binding lectins. In the present study, we evaluated the antiviral activity of seven plant-derived lectins with diverse glycan specificity and a lectin-rich leek extract. Four lectins and the leek extract showed antiviral properties against SARS-CoV-2 in A549-ACE2 cells with the Con A lectin being most potent while having low cytotoxicity. Con A showed an IC_{50} value of ~13 nM in A549-ACE2 cells that is comparable to the most potent anti-SARS-CoV-2 lectins, FRIL (~7 nM) and H84T-BanLec (~6 nM), and outcompetes remdesivir (~250–620 nM in our experiments) – one of the first drugs authorized for COVID-19 treatment. Con A exhibited broad antiviral activity against all six tested SARS-CoV-2 variants, including the predominant Omicron variant, and proved to be highly potent also in Calu-3 cells. We suggest that Con A forms a coat around virions and causes their aggregation, thereby preventing entry into the host cell. Furthermore, we demonstrated that *d*STORM is a powerful approach to study single-virus particles and the relative position of virion interactors, such as lectins.

4.1. Mode-of-action

After we identified initial candidates with antiviral properties, we first set out to investigate the mechanisms by which various lectins affect the infection cycle of SARS-CoV-2. Results from time-of-drug-addition experiments suggest that Con A, the lectin that showed highest antiviral efficacy, acted at early steps of the SARS-CoV-2 infection cycle and that its inhibitory effect cannot be attributed to its early interaction with Calu-3 cells. This was supported by imaging experiments (*d*STORM) that revealed that Con A coated and agglutinated virions (Fig. 7). Recent research conducted by Coa et al. (Cao et al., 2021) utilized magnetic beads coated with Con A to isolate SARS-CoV-2 virions, confirming a direct interaction between the lectin and the surface of SARS-CoV-2. Our observation of Con A-induced agglutination of SARS-CoV-2 is corroborated by an early study reporting similar cross-linking effects of Con A on hemagglutinating encephalomyelitis virus, another coronavirus family member (Greig and Bouillant, 1977). This suggests a virucidal effect mediated by virus agglutination as a contributing factor to the mode of action. Therefore, to further investigate the role of virus clumping, we tested the antiviral activity of the divalent succ-Con A, a chemically modified variant of Con A, that was reported for its lower agglutinating capability (Gunther et al., 1973). Succ-Con A showed a four times higher IC_{50} of 23.45 ± 8.20 μg/ml. A very similar result (IC_{50}: 33.8 ± 3.9 μg/ml) was revealed in a recent study by Wang and colleagues where succ-Con A was tested for its anti-SARS-CoV-2 properties using a pseudovirus assay and 293-ACE2 cells (Wang et al., 2021). These observations support the assumption that the antiviral activity of Con A is enhanced by its agglutinating properties (Fig. 7B). However, the difference in agglutinating properties of Con A and succ-Con A is not reflected in the Hill coefficients arguing that the dimeric form predominantly found for succ-Con A could be sufficient for high agglutinating properties. Alternatively, the cooperative mode of action could be attributed to effects beyond agglutination.

PSA is another dimeric lectin with a lower valence compared to Con A, while featuring overlapping sugar specificities (Barre et al., 2021). Indeed, at Calu-3-produced SARS-CoV-2 virions PSA exhibited a signal that was comparable to Con A as assessed by super-resolution microscopy. However, it did not show SARS-CoV-2 inhibition in virus assays, which could be due to the reduced ability of the bivalent PSA to agglutinate virions. Thus, collectively our findings suggest that the virus agglutinating properties of a lectin, rather than its interaction with the virus alone, may contribute to the inhibition of SARS-CoV-2 infection.

In vitro HHA treatment of both, A549-ACE2 and Calu-3 cells infected with SARS-CoV-2 resulted in measurable inhibition. At the same time, super-resolution microscopy did not reveal spatial proximity to virions. Our time-of-drug-addition revealed that HHA exhibited antiviral activity both at early steps of infection but also when it was added 2 and 6 h after infection. Previous time-of-addition studies with HHA tested against SARS-CoV in Vero E6 cells showed highest inhibitory effect around 5 h after infection (Keyaerts et al., 2007). Together with our super-resolution data revealing HHA signal at clathrin-free regions of A549-ACE2 cells, this points towards HHA-mediated inhibition at several steps: during docking and after endocytosis, but also at later steps in the viral life cycle such as virion assembly and maturation, e.g. by interfering with the endoplasmic reticulum-Golgi intermediate compartment (ERGIC). Further super-resolution experiments with ER, Golgi, and ERGIC markers and functional analyses could help to prove this hypothesis.

UDA showed a moderate antiviral effect in all *in vitro* experiments in A549-ACE2 cells and in three out of eight experiments in Calu-3 cells.

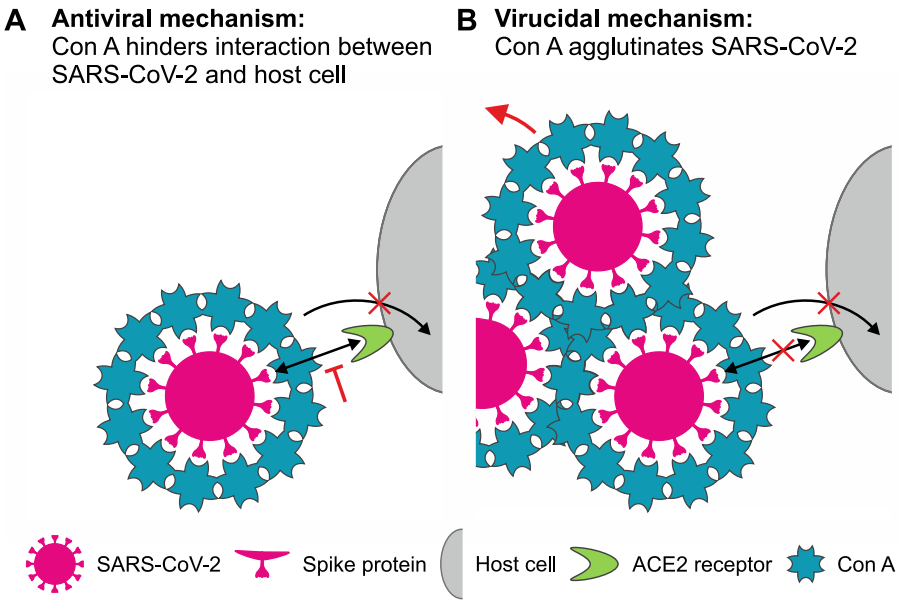

Fig. 7. Two mechanisms proposed for Con A-mediated SARS-CoV-2 inhibition. (A) Con A may block interaction between SARS-CoV-2 and the host cell (red blunt inhibition arrow ⊤) presumably via a direct interaction with mannose moieties at the spike protein. This would impede the downstream entry of the virus into the host cell, indicating an antiviral mechanism. (B) Interaction of multivalent Con A leads to the agglutination of SARS-CoV-2 virions, which could lead to an enhanced virus clearance (red arrow), suggesting a primarily virucidal mechanism. It is possible that Con A operates through a dual (A, B) mode-of-action. Please note that virus, lectin, cell, and receptor dimensions are not to scale.

UDA is a lectin that is also specific for N-acetyl-D-glucosamine and high-mannose type glycans (Itakura et al., 2017). Interestingly, super-resolution imaging revealed only a subtle signal in spatial proximity to SARS-CoV-2. This aligns with previous studies of the inhibitory effect of UDA against SARS-CoV (Keyaerts et al., 2007; Kumaki et al., 2011) and recent report on effectivity against SARS-CoV-2 in air-liquid-interface cultures (Vanhulle et al., 2022). Time-of-drug-addition experiments by Kumaki et al. conducted in Vero 76 cells infected with SARS-CoV revealed that UDA pre-treatment of cells and UDA pre-treatment of SARS-CoV resulted in comparably low IC_{50} concentrations, suggesting that UDA interacts with both cells and virions at early steps of infection. In conjunction with the very low UDA signal at SARS-CoV-2 particles and to Calu-3 cells compared to a more pronounced staining at virions located at the surface of Calu-3 cells, we hypothesize that UDA might act at the interface between the S1 RBD and host cell receptors. Recent reports confirmed direct attachment of UDA to SARS-CoV-2 via *in silico* ELISA experiments (Sabzian-Molaei et al., 2022). Interestingly, cell fusion experiments revealed that fusion between spike protein-expressing HEK293T cells or A549-ACE2 cells individually pretreated with UDA resulted in comparable or lower (in case of a post-application washing step) inhibition levels of fusion between these cells compared to a *concomitant* UDA treatment of HEK293T-spike cells and A549-ACE2 cells; and addition of UDA did not reduce the binding strength between RBD and ACE2 in surface plasmon resonance experiments (Vanhulle et al., 2022). Taken together, our and previous findings argue for a possible synergy between the ACE2 receptor and the RBD that is required for UDA's efficient integration at the ACE2-RBD interface, enabling its antiviral action. Further research is needed to clarify how exactly UDA exerts its antiviral effect.

WGA showed no antiviral activity in Calu-3 and A549 cells despite binding to viral particles generated in A549 cells. This is in contrast to two other recent studies that reported an inhibitory activity of WGA against SARS-CoV-2 (Auth et al., 2021) and its pseudoviral derivative (Wang et al., 2021). One possible explanation for these inconsistencies could be that WGA targets various types of glycans by recognizing N-acetyl-D-glucosamine found at starting points of almost all types of N-linked glycosylation as well as sialic acid. Thus, selective binding to the RBD of the spike protein is unlikely. Due to this broad specificity, WGA could at the same time exhibit inhibitory and infection-promoting effects via cross-linking the viral envelope and the glycocalyx of host cells. This can result in a fragile balance where small differences in glycosylation profile of cells and in experimental conditions can easily leverage between pronounced antiviral effect, no effect, or even adverse effects.

4.2. *Inhibitory effect of many lectins differs strongly between cell lines*

We observed considerable differences in antiviral properties of lectins in two lung epithelial cell lines, A549-ACE2 and Calu-3, with most lectins showing reduced antiviral activity in Calu-3 cells. This could be explained by the two different SARS-CoV-2 entry pathways that were previously proposed for these two cell lines (Jackson et al., 2022). A549-ACE2 cells do not express TMPRSS2, which precludes direct fusion with the plasma membrane and results in SARS-CoV-2 entry via endosome-mediated endocytosis that is promoted by ACE2 (Koch et al., 2021). In this pathway, the S1 subunit shedding is realized in the acidic environment of endolysosomes by another protease, cathepsin L, and is also likely assisted by interaction with ACE2. In contrast, Calu-3 cells express TMPRSS2 that upon conformational changes of the spike protein induced by ACE2 can shed the S1 subunit of the spike protein leading to the exposure of the fusion peptide in the S2 subunit and triggering virus entry via fusion with the plasma membrane directly after virion binding. Thus, while in Calu-3 cells lectins appear to attenuate or preclude the interaction between the S1 subunit and the ACE2 receptor at the cell surface, in A549-ACE2 cells lectins might interfere dually: (1) at the cell surface by reducing endocytosis and (2) in endolysosomes by reducing the probability of S1 shedding and thus membrane fusion. In the latter case, the effects could multiply, explaining the enhanced antiviral properties of some lectins that we observed in A549-ACE2 cells.

Another difference between A549 and Calu-3 cells is the higher Mucin 1 expression in the latter (Berger et al., 1999), possibly resulting in a mucus layer with an overall higher level of glycosylation. While Mucin 1 expression had no effect on SARS-CoV-2 replication (Kim et al., 2021), a possibly thicker mucus layer with the highly glycosylated Mucin 1 could sequester various lectins (e.g. via direct interaction of lectins with the sugar moieties of Mucin 1), preventing their interaction

with the spike protein.

When comparing our work with recent data on antiviral activity of lectins against SARS-CoV-2, we also observed differences for WGA. While in our experimental settings, WGA did not show any considerable effect, studies in 293-ACE2 cells with pseudovirus (Wang et al., 2021) or in Vero B4 and to a lower extent in Calu-3 cells infected with authentic SARS-CoV-2 (Auth et al., 2021) revealed potent inhibitory activity. These discrepancies could be explained by the fact that the glycosylation footprint can substantially differ among cell types (Goh and Ng, 2018) and influence the glycosylation profile of the virus produced in these cells. This underlines the necessity for further studies where lectins with anti-SARS-CoV-2 properties are applied to a broad range of cells, including alveolar type II epithelial cells.

4.3. Treatment concept

Previously, lectins have been proposed as potential therapeutic strategy for treatment of various viral infections, including of those with HIV, hepatitis C virus, and coronaviruses (reviewed in Mazalovska and Kouokam 2018). However, while a lectin-based treatment is not a sufficiently safe strategy against persistent viruses, in the case of acute viral infections like SARS-CoV-2, it might be a suitable option because when given early enough, it should lower viral load and thus, the likelihood for severe course of disease.

Interestingly, the impure leek extract showed a remarkable IC_{50} value of ~9 μg/ml in A549-ACE2 cells. This falls within the concentration range of lectin typically found in leek leaves (0.01 g/kg), which has been documented as nontoxic for mammals (Peumans and Van Damme, 1996). Presumably, the anti-viral effect was conferred by the leek lectin APA that has been previously reported to show exceptionally high inhibitory effects against SARS-CoV (Keyaerts et al., 2007). The observation that impure leek extract was sufficient to inhibit SARS-CoV-2 *in vitro* encourages further investigation of the leek extract and the contained APA lectin, which could provide a starting point for new prevention and treatment strategies.

Despite Con A displaying significant inhibitory effects against SARS-CoV-2 with minimal cytotoxicity in our assays, *in vitro* results may not fully capture potential *in vivo* adverse effects, including immune reactions. Importantly, Con A is known for its mitogenic effects on lymphocytes (see Ashraf and Khan, 2003 for review) induced by its cross-linking interactions with T cell receptors (Schneider et al., 2012), highlighting such concerns. Previous studies in rodents demonstrated that intravenous injection of high doses (20 mg/kg) of Con A can induce T cell-mediated liver injury (Heymann et al., 2015; Trautwein et al., 1998) and infusion of 20 mg/ml Con A for 50 min into the lung led to morphological deformation in alveolar epithelial cells (Welsch and Schumacher, 1983). However, the dosages employed in these experiments are orders of magnitude higher compared to the IC_{50} values we measured for Con A. Although developing engineered lectins on the basis of Con A that retain their virucidal agglutinating properties without T cell receptor cross-linking is warranted, we note that a topical application of Con A such as nose spray should further reduce the risk of T cell-mediated side-effects.

In fact, considering the potential drawbacks of injections and infusions, intranasal application of lectins emerges as a more viable strategy against COVID-19, and acute respiratory infections in general. Studies highlighting that the adverse effects of Con A are highly dependent of the administration route, with subcutaneous and intraperitoneal applications showing the least toxicity, lend further support to the topical application of lectins (reviewed in Ballerstadt et al., 2006). Importantly, multiple research teams have shown that nose sprays containing different compounds, including the engineered banana lectin H84T-BanLec, can effectively prevent and reduce SARS-CoV-2 infection in animals (Chan et al., 2022; de Vries et al., 2021; Shapira et al., 2022). Thus, intranasal application of lectins preventing SARS-CoV-2 infection and approved for clinical use could provide an effective prophylactic or therapeutic option against COVID-19. To advance lectins as antiviral agents, assessing the safety of their topical administration to mucosal tissues is crucial.

5. Conclusion

Overall, our study demonstrates that multiple lectins with specificity for high-mannose glycans inhibit SARS-CoV-2 replication in lung epithelial cells via different mechanisms. Super-resolution microscopy revealed the spatial association of lectins and the virus and together with infection assays allowed profiling of different lectins in their antiviral activity. Taken together, these results support intranasal application of lectins to prevent SARS-CoV-2 infections. However, further research is required to comprehensively evaluate the safety of non-invasive administration of lectins.

6. Limitations of the study

The limitations of this study mostly pertain to the nature of used cell lines. Firstly, the cell lines used in this study are cancer-derived. Cancer cell lines often show deregulated glycosylation patterns compared to healthy non-malignant cells (Peixoto et al., 2019; Pinho and Reis, 2015; Wiersma, 2020). Therefore, the cytotoxic effect measured for the lectins used here might be an overestimation compared to native non-cancer epithelial cells. Furthermore, the potentially increased glycosylation of the mucus and the surface of cancer cells might compete for lectin binding to the spike protein and therefore the antiviral effect of lectins could be underestimated compared to non-cancer lung epithelial cells. Secondly, although we used human lung-derived epithelial cells, these cells do not fully represent an authentic cell system. In particular, given that glycosylation of viral proteins is conferred by the glycosylation machinery of the host cell, assessing the relevance of these findings to natural isolates is crucial. Further investigation using air-liquid interface cell cultures, particularly alveolar type II epithelial cells, is needed to confirm the universal inhibitory potential of selected lectins against SARS-CoV-2.

CRediT authorship contribution statement

Maja Klevanski: Writing – review & editing, Writing – original draft, Visualization, Validation, Supervision, Project administration, Methodology, Investigation, Formal analysis, Data curation, Conceptualization. **Heeyoung Kim:** Writing – original draft, Visualization, Methodology, Investigation, Formal analysis, Data curation. **Mike Heilemann:** Writing – review & editing, Funding acquisition. **Thomas Kuner:** Writing – review & editing, Supervision, Resources, Funding acquisition, Data curation, Conceptualization. **Ralf Bartenschlager:** Writing – review & editing, Supervision, Resources, Project administration, Funding acquisition, Conceptualization.

Declaration of competing interest

The authors declare that they have no known competing financial interests or personal relationships that could have appeared to influence the work reported in this paper.

Data availability

Data will be made available on request.

Acknowledgments

We gratefully thank Michaela Kaiser for excellent technical assistance. Work by R.B. was supported by the Deutsche Forschungsgemeinschaft (DFG) – Project Number 240245660 – SFB1129, and by the project "Virological and immunological determinants of

COVID-19 pathogenesis – lessons to get prepared for future pandemics (KA1-Co-02 "COVIPA")", a grant from the Helmholtz Association's Initiative and Networking Fund. M.H. gratefully acknowledges funding by the DFG (grants CRC1507 and RTG2556). We acknowledge the data storage service SDS@hd, supported by the Ministry of Science, Research and the Arts Baden-Württemberg (MWK) and the DFG through grant INST 35/1314-1 FUGG.

Appendix A. Supplementary data

Supplementary data to this article can be found online at https://doi.org/10.1016/j.antiviral.2024.105856.

References

Ashraf, M.T., Khan, R.H., 2003. Mitogenic lectins. Med. Sci. Mon. Int. Med. J. Exp. Clin. Res. 9, RA265–R269.

Auth, J., Fröba, M., Große, M., Rauch, P., Ruetalo, N., Schindler, M., Morokutti-kurz, M., Graf, P., Dolischka, A., Prieschl-grassauer, E., Setz, C., Schubert, U., 2021. Lectin from triticum vulgaris (WGA) inhibits infection with SARS-CoV-2 and its variants of concern alpha and beta. Int. J. Mol. Sci. 22 https://doi.org/10.3390/ijms221910205.

Ballerstadt, R., Evans, C., McNichols, R., Gowda, A., 2006. Concanavalin A for in vivo glucose sensing: a biotoxicity review. Biosens. Bioelectron. 22, 275–284. https://doi.org/10.1016/j.bios.2006.01.008.

Barre, A., Van Damme, E.J.M., Simplicien, M., Le Poder, S., Klonjkowski, B., Benoist, H., Peyrade, D., Rougé, P., 2021. Man-specific lectins from plants, fungi, algae and cyanobacteria, as potential blockers for SARS-CoV, MERS-CoV and SARS-CoV-2 (COVID-19) coronaviruses: Biomedical perspectives. Cells 10, 1–36. https://doi.org/10.3390/cells10071619.

Beheiry, M. El, Dahan, M., 2013. ViSP: representing single-particle localizations in three dimensions. Nat. Methods 10, 689–690. https://doi.org/10.1038/nmeth.2566.

Berger, J.T., Voynow, J.A., Peters, K.W., Rose, M.C., 1999. Respiratory carcinoma cell lines MUC genes and glycoconjugates. Am. J. Respir. Cell Mol. Biol. 20, 500–510. https://doi.org/10.1165/ajrcmb.20.3.3383.

Cao, C., Cai, Z., Xiao, X., Rao, J., Chen, J., Hu, N., Yang, M., Xing, X., Wang, Y., Li, M., Zhou, B., Wang, X., Wang, J., Xue, Y., 2021. The architecture of the SARS-CoV-2 RNA genome inside virion. Nat. Commun. 12, 1–14. https://doi.org/10.1038/s41467-021-22785-x.

Casalino, L., Gaieb, Z., Goldsmith, J.A., Hjorth, C.K., Dommer, A.C., Harbison, A.M., Fogarty, C.A., Barros, E.P., Taylor, B.C., McLellan, J.S., Fadda, E., Amaro, R.E., 2020. Beyond shielding: the roles of glycans in the SARS-CoV-2 spike protein. ACS Cent. Sci. 6, 1722–1734. https://doi.org/10.1021/acscentsci.0c01056.

Chan, J.F.-W., Oh, Y.J., Yuan, S., Chu, H., Yeung, M.-L., Canena, D., Chan, C.C.-S., Poon, V.K.-M., Chan, C.C.-Y., Zhang, A.J., Cai, J.-P., Ye, Z.-W., Wen, L., Yuen, T.T.-T., Chik, K.K.-H., Shuai, H., Wang, Y., Hou, Y., Luo, C., Chan, W.-M., Qin, Z., Sit, K.-Y., Au, W.-K., Legendre, M., Zhu, R., Hain, L., Seferovic, H., Tampé, R., To, K.K.-W., Chan, K.-H., Thomas, D.G., Klausberger, M., Xu, C., Moon, J.J., Stadlmann, J., Penninger, J.M., Oostenbrink, C., Hinterdorfer, P., Yuen, K.-Y., Markovitz, D.M., 2022. A molecularly engineered, broad-spectrum anti-coronavirus lectin inhibits SARS-CoV-2 and MERS-CoV infection in vivo. Cell Reports Med 3, 100774. https://doi.org/10.1016/j.xcrm.2022.100774.

Cortese, M., Lee, J.Y., Cerikan, B., Neufeldt, C.J., Oorschot, V.M.J., Köhrer, S., Hennies, J., Schieber, N.L., Ronchi, P., Mizzon, G., Romero-Brey, I., Santarella-Mellwig, R., Schorb, M., Boermel, M., Mocaer, K., Beckwith, M.S., Templin, R.M., Gross, V., Pape, C., Tischer, C., Frankish, J., Horvat, N.K., Laketa, V., Stanifer, M., Boulant, S., Ruggieri, A., Chatel-Chaix, L., Schwab, Y., Bartenschlager, R., 2020. Integrative imaging reveals SARS-CoV-2-induced reshaping of subcellular morphologies. Cell Host Microbe 28, 853–866.e5. https://doi.org/10.1016/j.chom.2020.11.003.

Dawood, A.A., 2021. Glycosylation, ligand binding sites and antigenic variations between membrane glycoprotein of COVID-19 and related coronaviruses. Vacunas 22, 1–9. https://doi.org/10.1016/j.vacun.2020.09.005.

de Vries, R.D., Schmitz, K.S., Bovier, F.T., Predella, C., Khao, J., Noack, D., Haagmans, B. L., Herfst, S., Stearns, K.N., Drew-Bear, J., Biswas, S., Rockx, B., McGill, G., Dorrello, N.V., Gellman, S.H., Alabi, C.A., de Swart, R.L., Moscona, A., Porotto, M., 2021. Intranasal fusion inhibitory lipopeptide prevents direct-contact SARS-CoV-2 transmission in ferrets. Science 80, 1379–1382. https://doi.org/10.1126/science.abf4896, 371.

Duma, Z., Chuturgoon, A.A., Ramsuran, V., Edward, V., Naidoo, P., Mpaka-Mbatha, M. N., Bhengu, K.N., Nembe, N., Pillay, R., Singh, R., Mkhize-Kwitshana, Z.L., 2022. The challenges of severe acute respiratory syndrome coronavirus 2 (SARS-CoV-2) testing in low-middle income countries and possible cost-effective measures in resource-limited settings. Glob. Health 18, 5. https://doi.org/10.1186/s12992-022-00796-7.

Goh, J.B., Ng, S.K., 2018. Impact of host cell line choice on glycan profile. Crit. Rev. Biotechnol. 38, 851–867. https://doi.org/10.1080/07388551.2017.1416577.

Gong, Y., Qin, S., Dai, L., Tian, Z., 2021. The glycosylation in SARS-CoV-2 and its receptor ACE2. Signal Transduct. Targeted Ther. 6 https://doi.org/10.1038/s41392-021-00809-8.

Greig, A.S., Bouillant, A.M.P., 1977. Binding effects of concanavalin A on a coronavirus. Can. J. Comp. Med.

Gunther, G.R., Wang, J.L., Yahara, I., Cunningham, B.A., Edelman, G.M., 1973. Concanavalin A derivatives with altered biological activities. Proc. Natl. Acad. Sci. USA 70, 1012–1016. https://doi.org/10.1073/pnas.70.4.1012.

Harbison, A.M., Fogarty, C.A., Phung, T.K., Satheesan, A., Schulz, B.L., Fadda, E., 2022. Fine-tuning the spike: role of the nature and topology of the glycan shield in the structure and dynamics of the SARS-CoV-2 S. Chem. Sci. 13, 386–395. https://doi.org/10.1039/d1sc04832e.

Hashmi, S.K., Murad, M.H., Theel, E.S., 2020. Screening for SARS-CoV-2: health policy implications in low- and middle-income countries. Mayo Clin. Proc. 95, 2606–2608. https://doi.org/10.1016/j.mayocp.2020.10.007.

Heilemann, M., van de Linde, S., Schüttpelz, M., Kasper, R., Seefeldt, B., Mukherjee, A., Tinnefeld, P., Sauer, M., 2008. Subdiffraction-resolution fluorescence imaging with conventional fluorescent probes. Angew. Chem. Int. Ed. 47, 6172–6176. https://doi.org/10.1002/anie.200802376.

Helmerich, D.A., Beliu, G., Taban, D., Meub, M., Streit, M., Kuhlemann, A., Doose, S., Sauer, M., 2022. Photoswitching fingerprint analysis bypasses the 10-nm resolution barrier. Nat. Methods 19, 986–994. https://doi.org/10.1038/s41592-022-01548-6.

Heymann, f., Hamesch, k., Weiskirchen, R., Tacke, F., 2015. The concanavalin A model of acute hepatitis in mice. Lab. Anim. 49, 12–20. https://doi.org/10.1177/0023677215572841.

Huang, L., Li, X., Gu, X., Zhang, H., Ren, L., Guo, L., Liu, M., Wang, Yimin, Cui, D., Wang, Yeming, Zhang, X., Shang, L., Zhong, J., Wang, X., Wang, J., Cao, B., 2022. Health outcomes in people 2 years after surviving hospitalisation with COVID-19: a longitudinal cohort study. Lancet Respir. Med. 10, 863–876. https://doi.org/10.1016/S2213-2600(22)00126-6.

Itakura, Y., Nakamura-Tsuruta, S., Kominami, J., Tateno, H., Hirabayashi, J., 2017. Sugar-binding profiles of chitin-binding lectins from the hevein family: a comprehensive study. Int. J. Mol. Sci. 18 https://doi.org/10.3390/ijms18061160.

Jackson, C.B., Farzan, M., Chen, B., Choe, H., 2022. Mechanisms of SARS-CoV-2 entry into cells. Nat. Rev. Mol. Cell Biol. 23, 3–20. https://doi.org/10.1038/s41580-021-00418-x.

Keyaerts, E., Vijgen, L., Pannecouque, C., Van Damme, E., Peumans, W., Egberink, H., Balzarini, J., Van Ranst, M., 2007. Plant lectins are potent inhibitors of coronaviruses by interfering with two targets in the viral replication cycle. Antivir. Res. 75, 179–187. https://doi.org/10.1016/j.antiviral.2007.03.003.

Kim, D., Maharjan, S., Kim, J., Park, S., Park, J.A., Park, B.K., Lee, Y., Kwon, H.J., 2021. MUC1-C influences cell survival in lung adenocarcinoma Calu-3 cells after SARS-CoV-2 infection. BMB Rep 54, 425–430. https://doi.org/10.5483/BMBRep.2021.54.8.018.

Klein, S., Cortese, M., Winter, S.L., Wachsmuth-Melm, M., Neufeldt, C.J., Cerikan, B., Stanifer, M.L., Boulant, S., Bartenschlager, R., Chlanda, P., 2020. SARS-CoV-2 structure and replication characterized by in situ cryo-electron tomography. Nat. Commun. 11, 5885. https://doi.org/10.1038/s41467-020-19619-7.

Klevanski, M., Herrmannsdoerfer, F., Sass, S., Venkataramani, V., Heilemann, M., Kuner, T., 2020. Automated highly multiplexed super-resolution imaging of protein nano-architecture in cells and tissues. Nat. Commun. 11, 1552. https://doi.org/10.1038/s41467-020-15362-1.

Koch, J., Uckeley, Z.M., Doldan, P., Stanifer, M., Boulant, S., Lozach, P., 2021. TMPRSS2 expression dictates the entry route used by SARS-CoV-2 to infect host cells. EMBO J. 40, 1–20. https://doi.org/10.15252/embj.2021107821.

Kumaki, Y., Wandersee, M.K., Smith, A.J., Zhou, Y., Simmons, G., Nelson, N.M., Bailey, K.W., Vest, Z.G., Li, J.K.K., Chan, P.K.S., Smee, D.F., Barnard, D.L., 2011. Inhibition of severe acute respiratory syndrome coronavirus replication in a lethal SARS-CoV BALB/c mouse model by stinging nettle lectin, Urtica dioica agglutinin. Antivir. Res. 90, 22–32. https://doi.org/10.1016/j.antiviral.2011.02.003.

Kuo, C.F., Wang, Y.H., Lei, H.Y., Wang, C.H., Tsao, N., 2007. Concanavalin A protects mice from a lethal inoculation of intragastric Klebsiella pneumoniae and reduces the induced liver damage. Antimicrob. Agents Chemother. 51, 3122–3130. https://doi.org/10.1128/AAC.01379-06.

Laemmli, U.K., 1970. Cleavage of structural proteins during the assembly of the head of bacteriophage T4. Nature 227, 680–685. https://doi.org/10.1038/227680a0.

Lardone, R.D., Garay, Y.C., Parodi, P., de la Fuente, S., Angeloni, G., Bravo, E.O., Schmider, A.K., Irazoqui, F.J., 2021. How glycobiology can help us treat and beat the COVID-19 pandemic. J. Biol. Chem. 296 https://doi.org/10.1016/j.jbc.2021.100375.

Laue, M., Kauter, A., Hoffmann, T., Möller, L., Michel, J., Nitsche, A., 2021. Morphometry of SARS-CoV and SARS-CoV-2 particles in ultrathin plastic sections of infected Vero cell cultures. Sci. Rep. 11, 1–11. https://doi.org/10.1038/s41598-021-82852-7.

Levet, F., Julien, G., Galland, R., Butler, C., Beghin, A., Chazeau, A., Hoess, P., Ries, J., Giannone, G., Sibarita, J.B., 2019. A tessellation-based colocalization analysis approach for single-molecule localization microscopy. Nat. Commun. 10, 1–12. https://doi.org/10.1038/s41467-019-10007-4.

Liu, Y.M., Shahed-Al-Mahmud, M., Chen, X., Chen, T.H., Liao, K.S., Lo, J.M., Wu, Y.M., Ho, M.C., Wu, C.Y., Wong, C.H., Jan, J.T., Ma, C., 2020. A carbohydrate-binding protein from the edible lablab beans effectively blocks the infections of influenza viruses and SARS-CoV-2. Cell Rep. 32, 108016 https://doi.org/10.1016/j.celrep.2020.108016.

Mallm, J.-P., Bundschuh, C., Kim, H., Weidner, N., Steiger, S., Lander, I., Börner, K., Bauer, K., Hübschmann, D., Benes, V., Rausch, T., Trevisan, N., De Azevedo, D., Telzerow, A., Laurence Jost, K., Parthé, S., Schnitzler, P., Boutros, M., Müller, B., Bartenschlager, R., Kräusslich, H.-G., Rippe, K., 2021. Local emergence and decline of a SARS-CoV-2 variant with mutations L452R and N501Y in the spike protein. medRxiv. https://doi.org/10.1101/2023.10.12.23296928, 2021.04.27.21254849.

Mazalovska, M., Kouokam, J.C., 2018. Lectins as promising therapeutics for the prevention and treatment of HIV and other potential coinfections. BioMed Res. Int. https://doi.org/10.1155/2018/3750646, 2018.

Peixoto, A., Relvas-Santos, M., Azevedo, R., Lara Santos, L., Ferreira, J.A., 2019. Protein glycosylation and tumor microenvironment alterations driving cancer hallmarks. Front. Oncol. 9, 1–24. https://doi.org/10.3389/fonc.2019.00380.

Peumans, W.J., Smeets, K., Van Nerum, K., Van Leuven, F., Van Damme, E.J.M., 1997. Lectin and alliinase are the predominant proteins in nectar from leek (Allium porrum L.) flowers. Planta 201, 298–302. https://doi.org/10.1007/s004250050070.

Peumans, W.J., Van Damme, E.J.M., 1996. Prevalence, biological activity and genetic manipulation of lectins in foods. Trends Food Sci. Technol. 7, 132–138. https://doi.org/10.1016/0924-2244(96)10015-7.

Pinho, S.S., Reis, C.A., 2015. Glycosylation in cancer: mechanisms and clinical implications. Nat. Rev. Cancer 15, 540–555. https://doi.org/10.1038/nrc3982.

Raub, T.J., Koroly, M.J., Roberts, R.M., 1990. Endocytosis of wheat germ agglutinin binding sites from the cell surface into a tubular endosomal network. J. Cell. Physiol. 143, 1–12. https://doi.org/10.1002/jcp.1041430102.

Reis, C.A., Tauber, R., Blanchard, V., 2021. Glycosylation is a key in SARS-CoV-2 infection. J. Mol. Med. 99, 1023–1031. https://doi.org/10.1007/s00109-021-02092-0.

Sabzian-Molaei, F., Nasiri Khalili, M.A., Sabzian-Molaei, M., Shahsavarani, H., Fattah Pour, A., Molaei Rad, A., Hadi, A., 2022. Urtica dioica Agglutinin: a plant protein candidate for inhibition of SARS-COV-2 receptor-binding domain for control of Covid19 Infection. PLoS One 17, e0268156. https://doi.org/10.1371/journal.pone.0268156.

Scherer, K.M., Mascheroni, L., Carnell, G.W., Wunderlich, L.C.S., Makarchuk, S., Brockhoff, M., Mela, I., Fernandez-Villegas, A., Barysevich, M., Stewart, H., Suau Sans, M., George, C.L., Lamb, J.R., Kaminski-Schierle, G.S., Heeney, J.L., Kaminski, C.F., 2022. SARS-CoV-2 nucleocapsid protein adheres to replication organelles before viral assembly at the Golgi/ERGIC and lysosome-mediated egress. Sci. Adv. 8 https://doi.org/10.1126/sciadv.abl4895.

Schneider, O.D., Millen, S.H., Weiss, A.A., Miller, W.E., 2012. Mechanistic insight into pertussis toxin and lectin signaling using T cells engineered to express a cd8α/cd3ζ chimeric receptor. Biochemistry 51, 4126–4137. https://doi.org/10.1021/bi3002693.

Shajahan, A., Pepi, L.E., Rouhani, D.S., Heiss, C., Azadi, P., 2021. Glycosylation of SARS-CoV-2: structural and functional insights. Anal. Bioanal. Chem. 413, 7179–7193. https://doi.org/10.1007/s00216-021-03499-x.

Shapira, T., Monreal, I.A., Dion, S.P., Buchholz, D.W., Imbiakha, B., Olmstead, A.D., Jager, M., Désilets, A., Gao, G., Martins, M., Vandal, T., Thompson, C.A.H., Chin, A., Rees, W.D., Steiner, T., Nabi, I.R., Marsault, E., Sahler, J., Diel, D.G., Van de Walle, G.R., August, A., Whittaker, G.R., Boudreault, P.L., Leduc, R., Aguilar, H.C., Jean, F., 2022. A TMPRSS2 inhibitor acts as a pan-SARS-CoV-2 prophylactic and therapeutic. Nature 605, 340–348. https://doi.org/10.1038/s41586-022-04661-w.

Steuten, K., Kim, H., Widen, J.C., Babin, B.M., Onguka, O., Lovell, S., Bolgi, O., Cerikan, B., Neufeldt, C.J., Cortese, M., Muir, R.K., Bennett, J.M., Geiss-Friedlander, R., Peters, C., Bartenschlager, R., Bogyo, M., 2021. Challenges for targeting SARS-CoV-2 proteases as a therapeutic strategy for COVID-19. ACS Infect. Dis. 7, 1457–1468. https://doi.org/10.1021/acsinfecdis.0c00815.

Storti, B., Quaranta, P., Di Primio, C., Clementi, N., Mancini, N., Criscuolo, E., Spezia, P. G., Carnicelli, V., Lottini, G., Paolini, E., Freer, G., Lai, M., Costa, M., Beltram, F., Diaspro, A., Pistello, M., Zucchi, R., Bianchini, P., Signore, G., Bizzarri, R., 2021. A spatial multi-scale fluorescence microscopy toolbox discloses entry checkpoints of SARS-CoV-2 variants in Vero E6 cells. Comput. Struct. Biotechnol. J. 19, 6140–6156. https://doi.org/10.1016/j.csbj.2021.10.038.

Trautwein, C., Rakemann, T., Malek, N.P., Plümpe, J., Tiegs, G., Manns, M.P., 1998. Concanavalin A-induced liver injury triggers hepatocyte proliferation. J. Clin. Invest. 101, 1960–1969. https://doi.org/10.1172/JCI504.

Vanhulle, E., D'huys, T., Provinciael, B., Stroobants, J., Camps, A., Noppen, S., Schols, D., Van Damme, E.J.M., Maes, P., Stevaert, A., Vermeire, K., 2022. Carbohydrate-binding protein from stinging nettle as fusion inhibitor for SARS-CoV-2 variants of concern. Front. Cell. Infect. Microbiol. 12, 1–18. https://doi.org/10.3389/fcimb.2022.989534.

Vetterlein, M., Ellinger, A., Neumüller, J., Pavelka, M., 2002. Golgi apparatus and TGN during endocytosis. Histochem. Cell Biol. 117, 143–150. https://doi.org/10.1007/s00418-001-0371-1.

Wang, J., Han, M., Roy, A.R., Wang, H., Möckl, L., Zeng, L., Moerner, W.E., Qi, L.S., 2022. Multi-color super-resolution imaging to study human coronavirus RNA during cellular infection. Cell Reports Methods 2. https://doi.org/10.1016/j.crmeth.2022.100170.

Wang, W., Li, Q., Wu, J., Hu, Y., Wu, G., Yu, C., Xu, K., Liu, X., Wang, Q., Huang, W., Wang, L., Wang, Y., 2021. Lentil lectin derived from Lens culinaris exhibit broad antiviral activities against SARS-CoV-2 variants. Emerg. Microb. Infect. 10, 1519–1529. https://doi.org/10.1080/22221751.2021.1957720.

Watanabe, Y., Allen, J.D., Wrapp, D., McLellan, J.S., Crispin, M., 2020. Site-specific glycan analysis of the SARS-CoV-2 spike. Science 369, 330–333. https://doi.org/10.1126/science.abb9983.

Welsch, U., Schumacher, U., 1983. In vivo binding and effects of Concanavalin A (Con A) on rat and mouse pulmonary alveolar epithelial cells and macrophages. Virchows Arch. B Cell Pathol. Incl. Mol. Pathol. 44, 45–56. https://doi.org/10.1007/BF02890158.

WHO Coronavirus, 2023. COVID-19). Dashboard [WWW Document]. https://covid19.who.int/.

Wiersma, V.R., 2020. Lectins as modulators of autophagy in cancer immunotherapy. In: Autophagy in Immune Response: Impact on Cancer Immunotherapy. Elsevier, pp. 53–74. https://doi.org/10.1016/B978-0-12-819609-0.00004-3.

Wolter, S., Schüttpelz, M., Tscherepanow, M., Van De Linde, S., Heilemann, M., Sauer, M., 2010. Real-time computation of subdiffraction-resolution fluorescence images. J. Microsc. 237, 12–22. https://doi.org/10.1111/j.1365-2818.2009.03287.x.

Wu, C.-T., Lidsky, P.V., Xiao, Y., Cheng, R., Lee, I.T., Nakayama, T., Jiang, S., He, W., Demeter, J., Knight, M.G., Turn, R.E., Rojas-Hernandez, L.S., Ye, C., Chiem, K., Shon, J., Martinez-Sobrido, L., Bertozzi, C.R., Nolan, G.P., Nayak, J.V., Milla, C., Andino, R., Jackson, P.K., 2023. SARS-CoV-2 replication in airway epithelia requires motile cilia and microvillar reprogramming. Cell 186, 112–130.e20. https://doi.org/10.1016/j.cell.2022.11.030.

Yang, Q., Hughes, T.A., Kelkar, A., Yu, X., Cheng, K., Park, S., Huang, W.-C., Lovell, J.F., Neelamegham, S., 2020. Inhibition of SARS-CoV-2 viral entry upon blocking N- and O-glycan elaboration. Elife 9, 1–44. https://doi.org/10.7554/eLife.61552.